Svalbard surface snowpack, Azzurra Spagnesia, Elena Barbaroa, *, Matteo Feltraccoa, Federico Scotoc, Marco Vecchiato, Massimiliano Vardè^{a,} Mauro Mazzola^a, François Burgay^{d,e}, Federica Bruschi^f, Clara Jule Marie Hoppe^g, Allison Bailey^g, Andrea Gambaro^{a,b}, Carlo Barbante^{a,b}, Andrea Spolaor^{a,b} ^a Institute of Polar Sciences - National Research Council of Italy (ISP-CNR), Via Torino 155, 30172, Venice, Italy b Department of Environmental Sciences, Informatics and Statistics, Ca' Foscari University of Venice, Via Torino 155, 30172, Venice, Italy ^c Institute of Atmospheric Sciences and Climate - National Research Council of Italy (ISAC-CNR), Campus Ecotekne, Lecce, 73100, Italy ^d Laboratory of Environmental Chemistry (LUC), Paul Scherrer Institut (PSI), Villigen, 5232, Switzerland ^e Oeschger Centre for Climate Change Research, University of Bern, Bern, 3012, Switzerland f Department of Chemistry, Biology and Biotechnology, University of Perugia, Via dell'Elce di Sotto 8, 06123, Perugia, g Alfred Wegener Institute, Helmholtz Centre for Polar and Marine Research, 27570 Bremerhaven, Germany Corresponding: Elena Barbaro (elena.barbaro@cnr.it)

Seasonal and interannual variability on the chemical composition of the

Definizione stile: Car. predefinito paragrafo

ha eliminato: Impact of Arctic Amplification

ha eliminato: in Svalbard

Abstract

33

34

35

36

37

38

39

40

41

42

43

44

45

46

47

48

49

50

51

52

53

54

55

56

57

58

59

60

61

62

63

64

Arctic Amplification (AA) is driving long-term changes in the Arctic climate system, including glacier ice melt, rapid sea ice decline, and alterations in atmospheric and geochemical processes, with consequences on the formation, transport, and chemical composition of aerosols and seasonal snowpack. Svalbard, particularly vulnerable to AA, provides a valuable site to assess changes in local environmental processes contributing to the seasonal snow chemical composition. From 2018 to 2021, sampling campaigns at the Gruvebadet Snow Research Site in Ny-Ålesund, in the North-West of the Svalbard Archipelago, captured the interannual variability in ionic and elemental impurities within surface snow, reflecting seasonal differences in atmospheric and oceanic conditions. Notably, warmer conditions prevailed in 2018-19 and 2020-21, contrasting with the relatively colder season of 2019-20. Our findings suggest that impurity concentrations in the 2019-20 colder season are impacted by enhanced sea spray aerosol production, likely driven by a larger extent of sea ice, and drier, windy conditions. This phenomenon was particularly evident in March 2020, when extensive sea ice was present in Kongsfjorden and around Spitsbergen due to an exceptionally strong cold stratospheric polar vortex and unusual Arctic Oscillation (AO) index positive phase. By comparing the snow chemical composition of the 2019-20 season with 2018-19 and 2020-21, we provide insights into the interplay between short-term meteorological variability and the long-term climatic impacts of AA in Svalbard, as well as associated shifts in aerosol production process.

1. Introduction

Chemical analysis of surface Arctic snow and ice can provide valuable comprehension of the composition of Arctic aerosols, its deposition, and exchange processes (Lai et al., 2017). These processes are influenced by a range of factors, including Arctic Amplification (AA) – a pronounced, long-term increase in near-surface air temperature observed since 1975 (Chylek et al., 2022). AA is recognized as an inherent characteristic of the global climate system, with multiple intertwined causes operating on a spectrum of spatial and temporal scales. These include, but are not limited to, changes in sea ice extent that impact heat fluxes between the ocean and the atmosphere, and water vapor that alters longwave radiation (Serreze and Barry, 2011). The Svalbard Archipelago is particularly sensitive to these effects due to the relatively low altitude of its main ice fields and its geographical location in the higher North Atlantic, where the impact of AA is especially pronounced (Spolaor et al., 2024). Therefore, in the 21st century, predicting and characterizing climate change in Svalbard is particularly crucial, as changes in near-surface air temperature, precipitation, and sea ice extent occur at an extremely high pace (Gjermundsen et al., 2020; Rantanen et al., 2022). The Svalbard region,

ha eliminato: leading to significant...riving long-term changes in the Arctic climate system, including glacier ice melting...elt, rapid sea ice decline, and alterations in atmospheric and geochemical processes in the Arctic regio

ha eliminato: is... particularly exposed...ulnerable to the AA, thus represents...rovides a relevant...aluable site in the Arctic ... o evaluate... ssess changes in local environmental processes contributing to the seasonal snow chemical composition. Sampling campaigns were conducted from...rom 2018 to 2021 ... sampling campaigns at the Gruvebadet Snow Research Site in Ny-Ålesund, in the North-West of the Svalbard Archipelago. During... captured the investigated years, ...nterannual variability of...n ionic and elemental impurities in...ithin surface snowpack has been associated to an alternation between relative warm years (...now, reflecting seasonal differences in atmospheric and oceanic conditions. Notably, warmer conditions prevailed in 2018-19,...and 2020-21), typical of the Arctic Amplification (AA) period, and ... contrasting with the relatively cold years (...older season of 2019-20), more similar to the pre-AA conditions. Our results indicate... Our findings suggest that impurity concentrations in the concentration of impurities during the...019-20 colder sampling ...eason is strongly dependent on the production of...re impacted by enhanced spray related ...erosol production, likely deriving ...riven by a larger extension...xtent of sea ice, and drier, windy conditions. Our findings were therefore linked to the presence of...his phenomenon was particularly evident in March 2020, when extensive sea ice was present in the...Kongsfjorden in March 2020, and more generally ...nd around Spitsbergen, resulting from the exceptional occurrence of a...due to an exceptionally strong and... cold wintry

ha eliminato: present an overview of the possible impact of AA on the Svalbard snowpack, and the related change in the

ha eliminato: , which may be variously

ha eliminato: the

ha eliminato:), a non-linear... — a pronounced, long-term increase in near-surface air temperatures...emperature observed from...ince 1975 to date ...Chylek et al., 2022). AA is recognized as an inherent characteristic of the changing...global climate system, with multiple intertwined causes operating on a spectrum of spatial and temporal scales. These include, but are not limited to, changes in sea ice extent that impact heat fluxes between the ocean and the atmosphere, and water vapor that alters longwave radiation (Serreze and Barry, 2011). The Svalbard Archipelago is particularly affected by AA...ensitive to these effects due to the relatively low altitude of its main ice fields and its geographical location in the higher North Atlantic, which make...here the effect...mpact of AA more significant

ha formattato

ha formattato: Inglese (Regno Unito)

located at the southern edge of the seasonal Arctic sea_cice zone, is characterized by a maritime climate with strong temperature variations during winter (Hansen et al., 2014; Barbaro et al., 2021). In the Arctic winter, the stratospheric polar jet fosters a high-atmospheric vorticity zone. This winter vortex typically acts as a strong barrier for the long-range transport of pollutants from mid-latitudes (Lawrence et al., 2020). However, it occasionally allows warm southern air to penetrate the region (Schoeberl and Newman, 2015). Additionally, Svalbard frequently experiences intense cyclonic storms in autumn and winter, which bring both heat and moisture from lower latitudes (Rinke et al., 2017). These intense meteorological variations, generally linked with a weaker polar vortex (Sobota et al., 2020; Salzano et al., 2023), favor long-range transport of aerosols to the archipelago, including pollutants from continental sources (Stohl et al., 2006b; Yttri et al., 2014a; Vecchiato et al., 2024;

D'Amico et al., 2024).

of recent climatic changes.

ha formattato: Inglese (Regno Unito)

Arctic snow captures dry and wet deposition and forms an archive that includes a range of seasonal chemical species such as major ions and trace elements, as well as human-made pollutants emitted into the Arctic atmosphere (Koziol et al., 2021). Ny-Ålesund is a well-monitored area and a natural laboratory for complex system observations, ideal for exploring both long-range contaminants from mid- to high-latitude regions of Eurasia and Canada (Nawrot et al., 2016; Song et al., 2020; Vecchiato et al., 2024; D'Amico et al., 2024), and local inputs from both natural processes and human settlement (Vecchiato et al., 2018). Previous research has extensively investigated the chemistry of Arctic snow and the exchange of inorganic species between the cryosphere and the atmosphere across multiple sites, including Barrow, Summit Greenland, Alert, Sodankylä, and over the Arctic Ocean during the MOSAiC expedition (e.g., Beine et al., 2003; Björkman et al., 2013; Jacobi et al., 2019). Specific studies in Ny-Ålesund and surrounding areas have explored the temporal and compositional aspects of the lower atmosphere (Stohl et al., 2006a; Eleftheriadis et al., 2009; Geng et al., 2010; Zhan et al.,

ha eliminato: 2022

ha eliminato:

ha eliminato: While previous research investigated the temporal and compositional aspects of the Ny-Ålesund

ha eliminato: the chemistry of Arctic snow and the exchange of inorganic species between cryosphere and atmosphere have been the subject of a relatively small number of studies or of specific events (Dommergue et al., 2010; Spolaor et al., 2013, 2019; Barbante et al., 2017).

In this study, we evaluate the surface snow concentration of ionic (Cl $^{\text{-}}$, Br $^{\text{-}}$, NO $_3$ $^{\text{-}}$, SO $_4$ 2 $^{\text{-}}$, MSA, Na $^{\text{+}}$,

2014; Feltracco et al., 2020, 2021; Turetta et al., 2021), though relatively few have addressed the

detailed seasonal dynamics of snow-atmosphere interactions in this region. Building on this existing

research, our study aims to enhance the understanding of these interactions, particularly in the context

NH₄+, K⁺, Ca²⁺) and elemental impurities (Li, Be, Mg, Al, Ca, V, Cr, Mn, Fe, Co, Ni, Cu, Zn, As, Se,

Rb, Sr, Ag, Cd, Sb, Cs, Ba, Tl, Pb, Bi, U) for the snow seasons between 2018-2021, at the Gruvebadet

Snow Research Site (GSRS) location, 1 km south of Ny-Ålesund, where clean and undisturbed snow

conditions are guaranteed throughout the whole sampling season.

The differences in average meteorological and climatological conditions across the studied seasons

ha formattato: Pedice

 $\textbf{ha eliminato:} \ \mathrm{far} \ \mathrm{from}$

are analysed to assess how sea ice extent, polar vortex, and Arctic Oscillation (AO) conditions influence the composition of surface snow in connection with the aerosol-producing and deposition processes in Kongsfjorden.

2. Methodology

247

248

249

250

251

252 253

254

255

256

257 258

259

262

263

264

266

267

268

269 270

271

272

273 274

275

276

278

2.1 Sampling and processing

Three sampling campaigns were conducted in Svalbard between 2018 and 2021, covering the period from October to May according to the onset of the snowpack formation and melting. Sample collection followed the protocol presented in Spolaor et al. (2019), further adopted by Bertò et al. (2021), where consecutive and adjacent sampling was carried in a 3x3 meters snow sampling area, within a clean sampling snowfield of 100 m wide. Each sample was collected 10 cm apart from the previous one, along a precise path. This method was designed to minimise the temporal variability between consecutive samples and reduce the impact of potential spatial variability (within the 5-15% range, according to Spolaor et al., 2019).

ha formattato: Inglese (Stati Uniti)

During the first sampling campaign, carried out from October 4th, 2018 to May 10th, 2019, 114 surface 260 snow samples were collected in a delimited snow field located ~ 100 m south of the "Dirigibile Italia 261

Station" in Ny-Ålesund (78.92° N 11.93° E, Ny-Ålesund, Svalbard). The surface snow was sampled

within the upper 3 cm, as this is the snow layer most influenced by the aerosol-cryosphere exchanges,

and, in case of snowfall, by deposition (Spolaor et al., 2018, 2021b). This choice also minimised the

265 effect of different physical snow conditions (density, crystal shape, and size).

Concurrently, additional 133 snow samples were collected at the Gruvebadet Snow Research Site

(GSRS) to evaluate the spatial variability with respect to the snow samples collected in Ny-Ålesund.

The GSRS is a clean-area located about 1 km south of Ny-Ålesund, nearby the Gruvebadet

Atmospheric Laboratory (GAL), dedicated to the chemical and physical monitoring of the seasonal

snowpack (Scoto et al., 2023; Fig. S1). Throughout the season, the sampling resolution varied based

on light conditions. During the polar night (from October to early March), snow sampling was carried

out daily at Ny-Ålesund, and every 3-5 days at the GSRS. With the beginning of the polar day, daily

sampling was conducted both in Ny-Ålesund and at the GSRS in March, and then continued only at

the GSRS until the end of the snow season in June due to the lower contamination of the site, more

distant from the fervent local activities. This sampling resolution overlap during March ensured a

good comparison of results in both snow fields (Fig. S2).

277 Starting from the second campaign, snow sampling activities were conducted only at the GSRS site,

since clean conditions of the field in Ny-Ålesund could not be guaranteed due to construction works.

The snow sampling was carried out from October 26th, 2019 to May 25th, 2020, with a total of 107 279

280 samples collected. The surface snow layer was sampled every 3-5 days during the polar night (until

February 24th, 2020), and daily from the beginning of the polar day until the end of the snow season. 281

- Consecutive samples represent the same snow layer in the absence of snowfall or wind drift/erosion.
- 283 However, factors such as snow aging, potential element re-emission, transformation, and dry
- deposition can introduce variability, making continuous monitoring essential. 284
- 285 Finally, during the third snow sampling campaign, lasting from October 27th, 2020 to June 15th, 2021,
- a weekly sampling was conducted at GSRS, with a total of 32 samples collected. 286
- 287 During snow sampling, the temperature and density of surface snow were measured, and the density
- of snow was calculated based on weighting a 100 cc cylinder. After collection, snow samples were 288
- 289 melted, and two different aliquots were obtained and stored in separate vials. In a 1.5 mL
- 290 polypropylene (PP) vial, 1 mL of sample was stored for ionic species, while another aliquot was
 - stored in a 5 mL LDPE vials for trace elements analysis. PP vials designated to ionic species analysis
- 291 were previously sonicated for 30 min in UltraPure Water (UPW) (18 M Ω cm⁻¹ at 25 °C) for 292
- 293 decontamination. LDPE vial used for trace elements analysis were instead conditioned with HNO3
 - 2% and sonicated for 30 min. All sample aliquots were stored at -20°C in dark conditions and
- 294
- transported to the Venice ISP-CNR laboratories. 295

282

301

302

305

306

307 308

309 310

311

312

- Furthermore, seawater temperatures and salinity at 10 m depth were also monitored in Kongsfjorden 296
- (Kb3; 78°57.228'N, 11°57.192'E) during 2019-2021 spring seasons, with data collected every 3-6 297
- 298 days (Assmy et al. 2023). Data was derived from Conductivity Temperature Depth (CTD) casts with
- 299 either a MiniSTD model SD-204 (SAIV A/S, Bergen, Norway) or a XR-620 CTD (RBR Ltd, Ottawa,
- 300 Canada). Combined casts of both instruments conducted in May 2020 and 2021 did not reveal
 - differences in temperature or salinity in the reported accuracy (two post comma digits).

2.2 Analysis of ionic species

The analysis of anionic species (Cl⁻, Br⁻, NO₃⁻, SO₄²-, MSA) was carried out using an ion 303

chromatograph (IC, Thermo Scientific DionexTM ICS-5000, Waltham, MA, USA) coupled with a 304

single quadrupole mass spectrometer (MS, MSQ PlusTM, Thermo Scientific, Bremen, Germany). The

separation was performed using an anionic exchange column (Dionex Ion Pac AS 19 2 mm ID × 250

mm length) equipped with a guard column (Dionex Ion Pac AG19 2 mm ID × 50 mm length). Sodium

hydroxide (NaOH), used as mobile phase, was produced by an eluent generator (Dionex ICS 5000EG,

Thermo Scientific). The NaOH gradient with a 0.25 mL min⁻¹ flow rate was: 0-6 min at 15 mM; 6-

15 min gradient from 15 to 45 mM; 15-23 min column cleaning with 45 mM; 23-33 min equilibration

at 15 mM. The injection volume was 100 µL. A suppressor (ASRS 500, 2 mm, Thermo Scientific)

removed NaOH before entering the MS source. The IC-MS operated with a negative electrospray

313 source (ESI) with a temperature of 500°C and a needle voltage of 3 kV. The other MS parameters are reported by Barbaro et al. (2017). The same IC system was simultaneously used to determine cationic 314 species (Na+, K+, Ca2+ and NH4+). However, Ca2+ was not measured within the samples collected 315 316 during the second campaign due to instrumental limitations. The separation occurred with a capillary cation-exchange column (Dionex Ion Pac CS19-4 mm 0.4 317 318 mm ID \times 250 mm length), equipped with a guard column (Dionex Ion Pac CG19–4, 0.4 mm ID \times 50 mm length), and the species were determined using a conductivity detector. Analytical blanks of 319 320 ultrapure water (> 18 M Ω cm) were included in the analysis, and the Method Detection Limit (MDL) was set to 3 times the standard deviation of the blank values. Checks for accuracy were made using 321 certified multi-element standard solutions for anions (Cl⁻, Br⁻, NO₃⁻, SO₄²⁻, no. 89886-50ML-F, Sigma 322 Aldrich) and cations (Na⁺, K⁺, Ca²⁺, no. 89316-50ML-F, Sigma Aldrich) at a concentration of 10 mg 323 $L^{-1} \pm 0.2\%$. The analytical precision was quantified as the relative standard deviation (RSD) for 324 325 replicates (n > 3) of standard solutions and was always < 10% for each ion.

2.3 Trace Elements analysis

- Twenty-six elements (Li, Be, Mg, Al, Ca, V, Cr, Mn, Fe, Co, Ni, Cu, Zn, As, Se, Rb, Sr, Ag, Cd, Sb,
- 328 Cs, Ba, Tl, Pb, Bi and U) were analyzed on samples previously melted and acidified to 2% v/v with
- 329 HNO₃ (UpA grade, Romil, UK) for 24 hours before analysis (Spolaor et al., 2018; Spolaor et al.,
- 330 2021a).

326

- 331 The analysis was performed using Inductively Coupled Plasma Mass Spectrometry (ICP-MS, iCAP
- 332 RQ, Thermo Scientific, US). The ICP-MS was equipped with an ASX-560 autosampler (Teledyne
- 333 Cetac Technologies), PolyPro PFE nebulizer, PFE cyclonic spray chamber thermostated at 2.7°C,
- sapphire injector, quartz torch and Ni cones. The acquisition was performed at 1550 W of plasma RF
- power in Kinetic Energy Discrimination (KED) high matrix mode, using He as collision gas (4.3
- 336 mL min⁻¹). Instrument parameters were optimized for best sensitivity in the whole mass range,
- minimum oxides (< 1%) and double charges (< 3%). Quantification was obtained by external
- calibration with multi-elemental standards prepared in ultrapure water (18 $M\Omega$ cm⁻¹ at 25° C) with
- 339 2% v/v ultrapure grade HNO₃ (UpA grade, Romil, UK), with a combination of certified level multi-
- 340 elemental solutions IMS-102 and IMS-104 from UltraScientific. Analytical quality control was
- performed by memory test blank (repeated analysis of ultrapure grade HNO₃ 2% v/v blank solution)
- 342 after each sample and calibration verification (repeated analysis of reference standards) every 11
- samples. More details are found in Spolaor et al., 2021a.

344 345

The Lagrangian particle dispersion model HYSPLIT (Draxler, 1998; Stein et al., 2015) was used to 347 determine the source region of air masses over Ny-Ålesund. This model has previously been shown 348 349 to be an effective tool for the prediction of transport pathways into and within the Arctic and Antarctic regions (Barbaro et al., 2015; Feltracco et al., 2021). The simulations were driven using 350 351 meteorological data from the Global Data Assimilation System (GDAS) one-degree archive, set the top of the model at 10000 m and the height source equal to the GSRS altitude. Back-trajectories were 352 353 calculated every 6 h, with a propagation time of 120 h for each sampling period, as suggested in

previous studies on atmospheric circulation in the same site (Feltracco et al., 2021). This approach 354 355

was used to ensure an envelope working for all investigated tracers. The resulting multiple trajectories

were based on the screen-plot analyses of total spatial variance.

The Ice Service provided by the Norwegian Meteorological Institute (NIS) was employed to analyse the weather conditions via remotely sensed data and to generate ice charts of Svalbard, ice-edge information, and sea surface temperatures trends. Sea ice extent variability in Kongsfjorden was evaluated based on dataset made available by Gerland et al. (2022).

Differences between the sampling campaigns were evaluated through the NCEP/NCAR Reanalysis data from NOAA Physical Sciences Lab's daily composites tool, used to calculate the near-surface air temperatures across the Northern Hemisphere from October to May.

2.5 Statistical procedures and Enrichment Factors (EFs) Analysis

367

346

356

357 358

359

360

361

362

363 364 365

366

368 369

370

371

372

373 374

375

376

377 378

379

Results below the limit of detection were assumed to be equal to 1/2 of Method Determination Limit (MDL) prior to perform statistical analysis, to approximate their likely level based on the data distribution curve (best approximated as log-normal for most of the studied variables) (George et al., 2021).

The Wilcoxon test was applied on data from the 2018-19 sampling campaign conducted at Ny-Ålesund and Gruvebadet to determine whether the difference between the population median and the hypothesized median of surface snow contamination level was statistically significant. This model assumes that the data is sampled from two matched or dependent populations, and data is assumed to be continuous. Because it is a nonparametric test, it does not require a particular probability distribution of the dependent variable in the analysis. Furthermore, Enrichment Factors (EFs) using Ba as a crustal element of reference (Widepohl, 1995; Spolaor et al., 2021a; Ruppel et al., 2023), were calculated to explore the mixed sources of the investigated elements. To complement the EFs

analysis, a Hierarchical Cluster Analysis (HCA) was performed using Ward's algorithm and

ha eliminato: Furthermore

Euclidean distances as clustering criteria, to determine the presence of some clusters and simplify the interpretation of the dataset.

3 Results

3.1 Comparison between concentration trends at Gruvebadet and Ny-Ålesund

The concentration variations between an undisturbed area in Ny-Ålesund village and GSRS sites were compared during the 2018-19 sampling campaign to better understand the effect of spatial variability between the two sampling sites. The concentration trends of Na⁺, as sea salt tracer, Pb as anthropogenic species, and Ca²⁺ as crustal tracer, are reported in Fig. S2, for both sampling sites. Although the difference in time resolution between sites is apparent in Fig. S2, the difference in concentration trends appears very low or negligible, except for sporadic peaks in sea salt and crustal tracers present in the Ny-Ålesund record from November to February. These peaks do not consistently correlate with positive temperature anomalies and precipitation events, as some occurred under low temperatures and without significant precipitation (e.g., January and early February), suggesting that other processes, such as long-range transport, wind-driven deposition, or dry deposition may also play a role (Fig. S2). Concordant Pb trends emerge at Ny-Ålesund and Gruvebadet, with the highest concentrations observed from February to May.

To evaluate the differences in concentration range and spatial distribution of surface snow impurity content, we applied the Wilcoxon test for the 2018-19 sampling period by comparing the distributions for positive and negative differences of the ranks of their absolute values. At a significance level of 0.01, the two distributions from GSRS and Ny-Ålesund sites were not statistically different for all the trace elements and most of the inspected ions.

For this reason, only the GSRS temporal trend has been considered throughout the manuscript, referring to ionic loads (mg m⁻²) instead of concentrations (ng g⁻¹), to highlight the seasonal trends of specific tracers. The ionic load is calculated as ionic concentrations multiplied by the density and the thickness of sampled strata.

3.2 Interannual trends of chemical species on the surface snow

Three consecutive snow seasons were evaluated to define the chemical composition of the surface snow in the Arctic site of GSRS. The sea salt ions $Cl^{-}(50\%)$, $Na^{+}(23\%)$ represent the most abundant species, followed by $SO_4^{2-}(11\%)$, Mg (7%), Ca (2%), Fe (1%) and Al (1%). Similar relative

ha eliminato: with few isolated

ha eliminato: for

ha eliminato: , following

ha eliminato: depth

ha eliminato: (Fig. S3),

abundances were also found in previous studies on the snow of the Svalbard Archipelago (Beaudon and Moore, 2009; Vega et al., 2015; Barbaro et al., 2021; Spolaor et al., 2021b).

Table 1 reports the average ionic loads of the most abundant (> 1%) species in the surface snow, considering three different seasons: autumn is defined until December 21st, winter until March 21st, and spring from then to the melt onset, identified by 5-6 consecutive days of negative snow accumulation. The average ionic loads of the less abundant (< 1%) species are reported instead in

Table S1.

Table 1. Average ionic loads of the most abundant (>1%) ionic and elemental species in the surface snow during each season of the three consecutive sampling campaigns. The standard deviation is shown in brackets, while in the case of nss-SO₄²⁻ the brackets represent the percentage of nss-SO₄²⁻ compared to the total SO₄²⁻. "n" indicates the number of samples considered for the calculation of the average.

mg m ⁻²	total	Cl-	Na ⁺	SO ₄ ² -	nss-SO ₄ ² -	Mg	Fe	Ca	NO ₃ -	K ⁺	NH ₄ ⁺
t 2018 (n. 22)	32	15	7	3	1	3	2	0.3	0.5	0.3	0.04
autumn 2018 (n=22)	(25)	(21)	(11)	(4)	(36%)	(3)	(5)	(0.3)	(0.5)	(0.4)	(0.03)
winter 2018-19 (n=41)	116	55	31	16	8	8	0.4	0.4	2	2	0.3
Willer 2016-19 (II=41)	(80)	(68)	(39)	(16)	(51%)	(8)	(0.3) 2 (3) 1 (1) 2	(0.3)	(2)	(2)	(0.3)
spring 2019 (n=51)	76	36	19	9	4	6	2	0.6	1	1	0.5
spring 2019 (n=31)	(50)	(43)	(24)	(9)	(48%)	(5)	(3)	(0.4)	(1)	(1)	(0.4)
autumn 2019 (n=15)	214	101	40	26	16	10	1	9	5	2	4
autumii 2019 (ii=13)	(98)	(71)	(53)	(20)	(61%)	(6)	(1)	(12)	(4)	(3)	(5)
winter 2019-20 (n=43)	339	159	79	41	21	16	2	9	3	3	7
willer 2019-20 (II=45)	(120)	(88)	(73)	(20)	(52%)	(8)	2 (5) 0.4 (0.3) 2 (3) 1 (1) 2 (5)	(10)	(2)	(4)	(8)
spring 2020 (n=49)	273	110	52	28	15	21	6	13	4	2	5
spring 2020 (n=49)	(132)	(91)	(77)	(25)	(53%)	(21)	0.4 (0.3) 2 (3) 1 (1) 2 (5) 6 (9) 1 (2) 0.2 (0.4) 4	(16)	(2)	(4)	(8)
autumn 2020 (n=6)	803	435	191	66	18	84	1	2	6	9	2
autumm 2020 (n=0)	(542)	(466)	(205)	(83)	(27%)	(165)	(2)	(5)	(11)	(10)	(2)
winter 2020-21 (n=13)	327	207	64	41	24	6	0.2	0.2	5	3	1
winter 2020-21 (n=13)	(203)	(194)	(48)	(36)	(60%)	(5)	(0.4)	(0.1)	(3)	(2)	(1)
spring 2021 (n=13)	181	107	36	16	7	9	4	1	3	2	1
spring 2021 (n=13)	(92)	(86)	(26)	(12)	(43%)	(10)	(7)	(2)	(2)	(2)	(1)

The average loads of the first sampling year were lower compared to the other campaigns (Fig. S3). High average loads were observed instead for Cl⁻ and Na⁺ in the top snowpack layer during the 2019-20 and 2020-21 winter seasons. The highest concentrations of sea salt species were found in autumn 2020 (Fig. 1), despite low snow accumulation in a period of relatively high precipitation (Table S3). This apparent contradiction can likely be attributed to the increased wind speeds during that time, which may have caused snow redistribution, thereby limiting accumulation despite the considerable precipitation.

The non-sea-salt sulphate (nss-SO₄²⁻), calculated using a seawater SO₄²⁻/Na⁺ mass ratio of 0.252

(Millero et al., 2008), was the most abundant fraction of the total <u>sulphate</u> in autumn 2019 and winter 2020-21, while in autumn 2018 and 2020 sea salt <u>sulphate</u> (ss-SO₄²) was the dominant fraction. No

ha eliminato: melt onset. The average loads of the first sampling year were lower compared to the other campaigns (Fig. S4).

ha eliminato: , with
ha eliminato: winters
ha eliminato: being rather similar. Higher values
ha eliminato: salts

ha eliminato: In general, the winter seasons showed the

ha eliminato: , but less
ha eliminato: was recorded

ha eliminato: period (Fig. 1).

ha eliminato: sulfate

ha eliminato: :

higher

ha eliminato: sulfate

clear predominance between the two fractions was achieved during the other investigated seasons (Table 1).

The abundance of all chemical species investigated is quite similar for all years (Fig. §3), although the sampling campaign 2019-20 showed higher percentage of calcium ranging between 3% and 5%, in contrast to the typical concentrations < 1% found in the other two campaigns.

3.3 Polar vortex and Arctic Sea ice extent in 2019-20

According to the 2023 survey conducted by the National Snow and Ice Data Center (NSIDC), the maximum extent of Arctic Sea ice since 2014 has been recorded in March 2020, with 14.73 million square kilometres of the Arctic Ocean surface, in a decadal trend characterized by a -2.53% of decline, due to the Arctic Amplification. Considering the Kongsfjorden area, the total sea ice extent varied from 63.94 km² in March 2019 to 129.81 km² in March 2020, and was with 46.26 km² lowest in March 2021 (Gerland et al., 2022). Specifications on Drift Ice (DI), Fast Ice (FI), and Open Water (OW) extent are reported in Table S2. The 2020 maximum sea ice extent followed the exceptionally strong and cold stratospheric polar vortex that took place in the Northern Hemisphere (NH) during the 2019-20 polar winter, together with low wave activity from the troposphere, which allowed the polar vortex to remain relatively undisturbed (Lawrence et al., 2020). Notably, the 2020 Arctic Sea ice extent is 16% and 9% higher than previous (2018-19) and following (2020-21) records (dataset NSIDC, NOAA). Lower surface air temperatures, reduced precipitations, higher wind speed (m sec-1), and minor mean snow height were observed during the 2019-20 winter season, attributed to the influence of a strong polar vortex triggered by a net positive Artic Oscillation (AO) phase. The 2020 anomalous AO index is displayed in Fig. \$4. Seasonal values of mean air temperatures (°C), mean precipitation (mm), maximum mean wind speed (m sec⁻¹) and mean snow depth (cm) during the three consecutive sampling campaigns are reported in Table S3. Temperature data were provided by the Norwegian Centre for Climate Services (NCCS), while sea ice extent data were supplied by National Snow and Ice Data Center (NSIDC). Seawater temperature data collected at 10 m depth at a midfjord station near Ny-Ålesund (Kb3) was found to be colder during 2020 compared to 2019 and 2021 spring seasons (Table S4). Although these temperatures were still above the freezing point for the observed salinity levels, they contributed to colder overall conditions in Kongsfjorden, supporting the formation and prolonged presence of sea ice when combined with cold atmospheric conditions.

4. Discussion

458

459

460

461

462

463 464

465

466

467

468

469

470 471

472

473

474

475

476

477

478

479

480

481 482

483

484

485

486

4.1 Ny-Ålesund seasonal and interannual trends variability in surface snow

ha eliminato: S5

 $\mbox{\bf ha}$ $\mbox{\bf eliminato:}$), appearing more similar to Arctic type than Arctic Amplification conditions.

ha eliminato: with respect

ha eliminato: typical AA conditions, were induced by

ha eliminato: cold

ha eliminato: , and recorded in the 2019-20 winter season

ha eliminato: S6

ha eliminato:), promoting

ha eliminato: formation of sea ice

ha eliminato: and

ha eliminato: its duration through the season, together

ha eliminato: Salinity data also revealed modest fluctuations across the considered seasons, showing a decrease of 0.35 psu in 2020 relative to 2019, and a decrease of 0.1 psu compared to 2021.

The three consecutive sampling campaigns conducted from 2018 to 2021 confirmed the dominance of sea salt input in the surface snow of Svalbard, due to the proximity of the Kongsfjord (Barbaro et al., 2021). The dominant ions are Na⁺, Cl⁻, and SO₄²-, associated with the scavenging precipitation of marine aerosol (Hodgkins and Tranter, 1998). The observed mean seasonal trends (Fig. §3) display the highest concentrations of marine species in autumn 2020, followed by 2020-21 and 2019-20 winter seasons. However, wintry concentrations are presumably linked to weakened (2019-20) or destroyed (2020-21) polar vortex (Fig. 1) and intense cyclonic storms, associated with anomalous warming events capable of transporting both heat and moisture from lower latitudes to Svalbard (Rinke et al., 2017). In addition to these factors, it is important to account for snow ablation or erosion by wind. The change in snow height (Δh) between consecutive sampling events provides valuable insights into such processes. A decrease in snow height signals ablation can indeed result from snow melting (under positive temperatures), snow aging, sublimation, or snow drift. In particular, when wind speeds exceed 5 m s⁻¹, the threshold commonly accepted for initiating snow drift and ablation episodes (Pomeroy, 1989), we can infer the snow erosion due to wind drift likely occurred (Fig. 1). This effect may explain some of the variability in snow ion concentrations, especially during intense storms or strong winds.

Autumn 2020 represents most likely an outlier, due to scarce precipitations (Fig. 2) that led to more concentrated impurities in the surface snow. Meanwhile, late spring 2020 saw a notable increase of typical marine ions (Na⁺, Cl⁻, Br-, MSA, SO₄²⁻) and geogenic elements (Al, Ca, Mn, Fe, Sr₂, compared to spring 2019 (Fig. 2). This increase may be attributed to the very close drift Arctic Sea ice presence in Kongsfjorden (Table S2), which reached its maximum extent in March 2020, due to lowtemperature anomalies and intensified atmospherically driven sea ice transport and deformation due to higher winter wind speeds (Fig. §5). These conditions likely enhanced the production of sea spray aerosols, which, when carried by winds, may have increased the deposition of marine species onto the snowpack. Such atmospheric and environmental factors appear to have significantly contributed to the observed peaks of marine and geogenic species during this period. Concurrently, an outstanding positive phase of the Arctic Oscillation (AO) in the troposphere (Fig. 1) was recorded in January-March 2020 (Lawrence et al., 2020; Dethloff et al., 2022). Although the entire period was remarkable, January and February featured as clear outliers in the historical timeseries (1950-2023) reported by the NOAA service, while March 2020 exhibited significantly elevated values but did not exceed the statistical threshold for outliers (Fig. S4).

ha eliminato: likely

ha eliminato: likely

ha eliminato: S4

ha eliminato: 1

ha eliminato: Concerning the

ha eliminato: season, higher concentrations

ha eliminato:) species deposited in late spring 2020,

ha eliminato: 2).

ha eliminato: due

ha eliminato: . Indeed, the formation of sea ice leads to the production of highly saline frost flowers and brine at both the sea ice-ocean and sea ice-atmosphere interface. Brine and frost flowers formed on the surface of sea ice can be lifted by winds and dispersed, thereby increasing the concentration of sea spray aerosol in the planetary boundary layer, and subsequently enhancing deposition over the snowpack. The maximum sea ice coverage in the fjord occurred in March 2020 was a consequence of

ha eliminato: S7), likely linked to the exceptional occurrence of a strong and cold stratospheric polar vortex

ha eliminato:), featuring

ha eliminato: an outlier

ha eliminato:

ha eliminato:

ha formattato: Tipo di carattere: 12 pt, Non Grassetto

Formattato: Allineato a sinistra, Interlinea: multipla 1,08

ha eliminato:

534 535

503

504

505

506

507 508

509 510

511 512

513 514

515 516

517

518

519

520

521

522

523

524

525

526

527

528

529

530

531

532

533

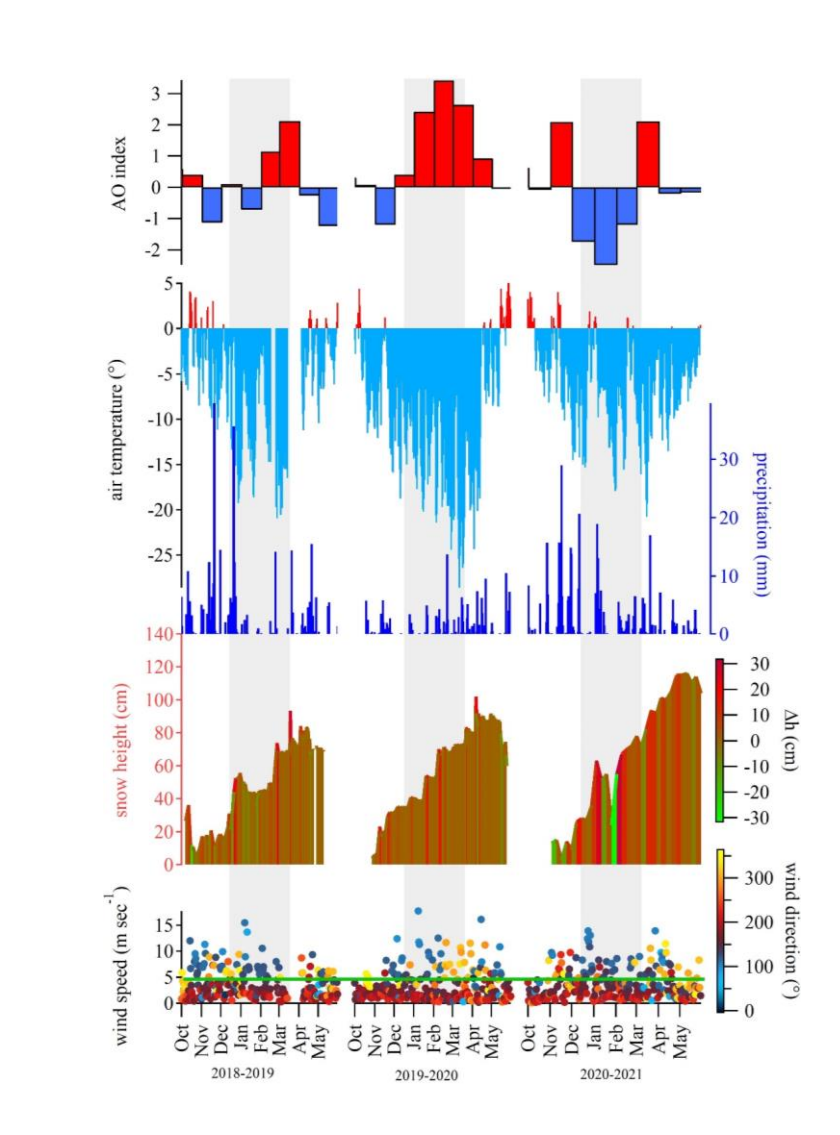


Figure 1. AO Index, air temperature (°C), precipitation (mm), snow height (cm), Δh snow height (cm), wind speed (m⁴ sec⁻¹), and wind direction (°) from the NCEP/NCAR Reanalysis data. The green horizontal line above the wind speed graph indicates the 5 m sec⁻¹ threshold, above which wind drift may occur on surface snow layers. The colour of the line refers to the Δh color scale, which indicates negative values of Δh, NOAA Physical Sciences Lab's daily composites tool was used to calculate the near-surface air temperatures across the Northern Hemisphere from October to May. Grey bands indicate the winter periods.

ha eliminato: Radiation (W m⁻²),

Formattato: Giustificato

604

605

606

607

A 2021 spring peak of marine species was also recorded, although more attenuated than <u>in spring</u> 2020 (Fig. 2, Fig. S3). This variation is likely attributable to different extents of sea ice in the fjord. Nonetheless, seawater temperatures in 2021, similar to those in 2020 and 2.3°C colder than in 2019 (Table S4), along with comparable wind speed conditions (Fig. S5), may also have contributed to the observed trends in marine species concentrations. Similarly, the spring peak of Mg, Sr, Mn, Fe, Al, and V in 2021 seems to reflect the high wind speed and positive AO index recorded from March to April 2021. Positive anomalies for air temperatures (A) and wind speed (W) conditions, together with negative anomalies in seawater (O) conditions were observed during the 2020-21 campaign, while negative A and O conditions were accompanied to positive W during 2019-20. On the contrary, 2018-19 diverges from the other campaigns for positive O condition associated to negative W condition anomalies. These observations provide valuable insights into how shifts in atmospheric and oceanic conditions impact the concentrations of ionic and elemental species in surface snow, enhancing our understanding of the underlying mechanisms that govern these changes in the context of AA conditions.

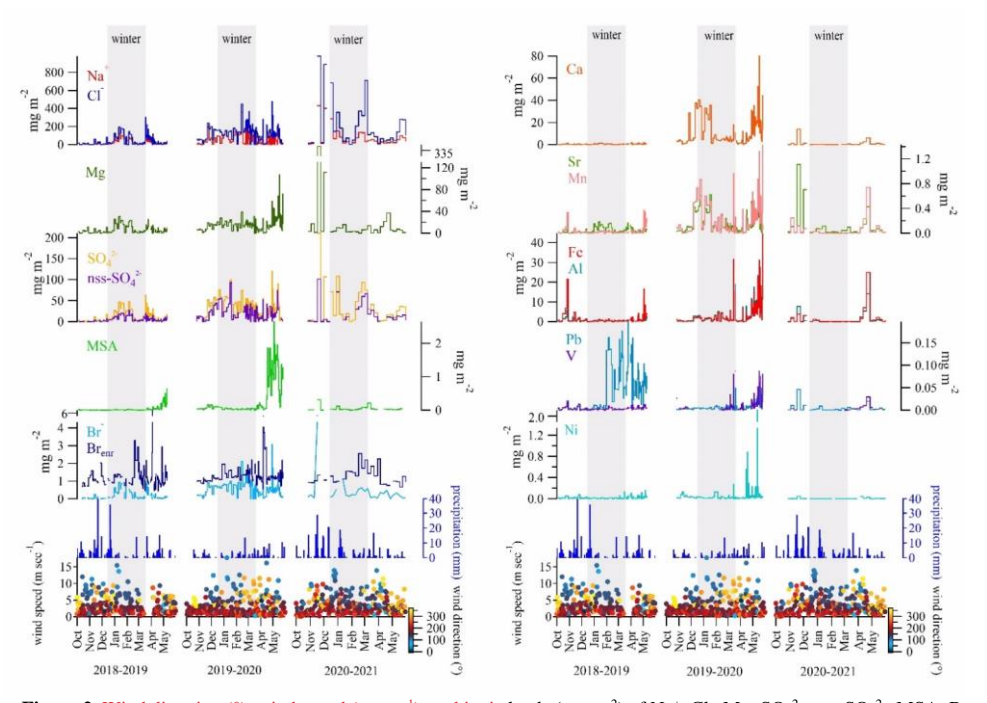


Figure 2. Wind direction (°), wind speed (m sec⁻¹), and ionic loads (mg m⁻²) of Na⁺, Cl⁻, Mg, SO₄²⁻, nss-SO₄²⁻, MSA, Br⁻, Ca, Sr, Mn, Fe, Al, Pb, V, Ni in the surface snow for the three sampling campaigns: 2018-19, 2019-20, 2020-21. Seasonal trends are here presented for specific elements to provide a detailed view of how concentrations vary across distinct sampling periods.

ha eliminato: <object>

ha eliminato: 1

ha eliminato: S4

ha eliminato: S7

ha eliminato: In particular, positive

ha eliminato: atmospheric

ha eliminato: oceanic

ha eliminato: findings highlight the complex interplay between

ha eliminato: patterns (AO and wind speed), local climate (temperature and sea ice extent).

ha eliminato: (SST, salinity), showing similar

ha eliminato: trends

ha eliminato: for wind, sea ice, and SST counterbalanced

ha eliminato:

ha eliminato: Ionic

A singular case is represented by Pb, which showed a 12.5-fold increase during winter-spring 2019, period compared to autumn 2018. The EF for Pb during these seasons exceeded 100, indicating a strong anthropogenic contribution. In contrast, the peak observed in 2020 no longer shows such elevated EF values (slightly above 10), suggesting a mixed source (Fig. 3). This implies that the April-May 2020 peak is largely of crustal origin, as the overlap with V (EF < 10) also suggests, possibly due to local dust events driven by strong winds exceeding the 5 m sec⁻¹ threshold (Fig. 2; Table S3).

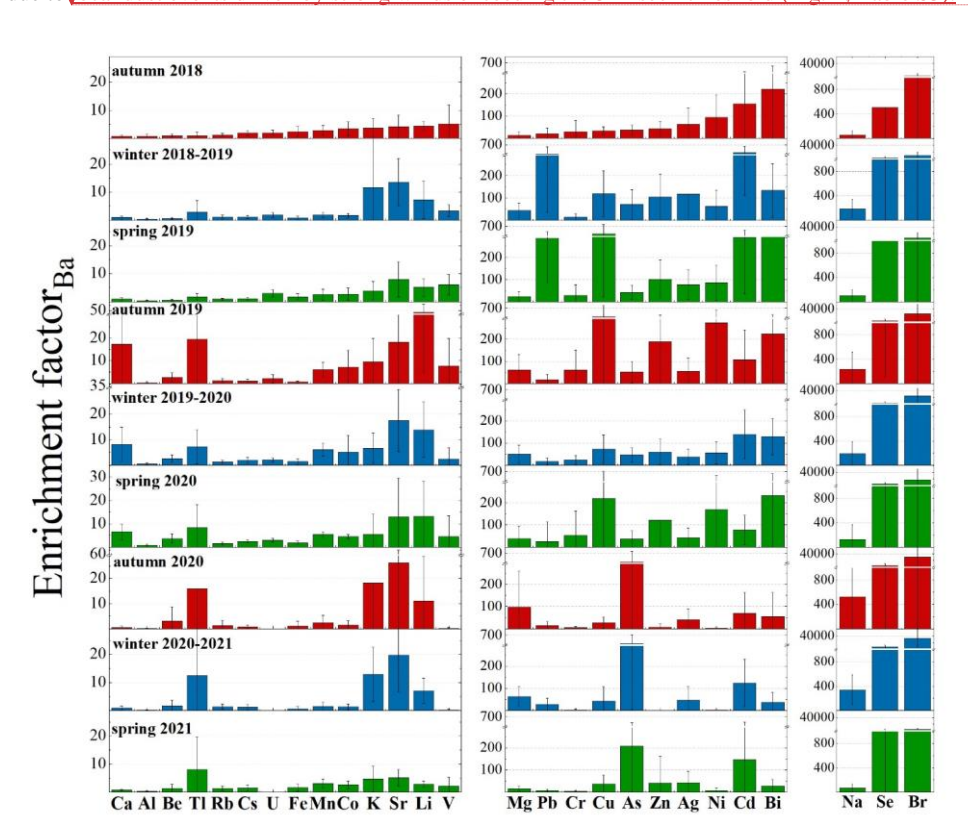


Figure 3. Enrichment Factors (EFs) calculated on all the presented trace elements for the three sampling campaigns: 2018-19, 2019-20, 2020-21. Calculating EFs for the full dataset offers a more robust assessment of potential sources and enrichment patterns, minimizing the variability inherent in individual seasons and allowing for a clearer distinction between crustal and non-crustal contributions.

The calculated EFs (Fig. 3) for Be, Al, V, Mn, Fe, Co, Rb, Cs, and U were consistently below 10, indicating a predominantly crustal (geogenic) origin for these elements. In contrast, Ni, and Sr displayed EFs greater than 10, suggesting contributions from mixed sources. Notably, Ni exhibited

ha eliminato: with remarkable trend concentration revealed

ha eliminato: . Generally,

ha eliminato: presents a typical seasonal variability in the Arctic aerosol, with higher wintry concentration caused by seasonal differences in the mixing conditions of the troposphere (Paatero et al., 2010). An accumulation in aerosol may lead to a prominent wet deposition in surface snow

ha eliminato: spring

ha eliminato: enhanced mixed-phase clouds' scavenging. The...

exceptionally high EF values – above 100 – during autumn 2019 and spring 2020 (Ni). Mixed sources were also recognised for Li, K, Cr, Cu, Zn, As, Ag, Cd, and Tl with occasional EF values over 100. This suggests significant anthropogenic contributions, especially for Cu (spring and autumn 2019; spring 2020), As (from autumn 2020 to spring 2021), Zn (autumn 2019) and Cd (from autumn 2018 to spring 2019; winter 2019-20).

648

649

650 651

652

653

654

655 656

657 658

659

660

661

662 663

664

665

666 667

668

669

670

671

672

673

674

675 676

677

678

The 2019 springtime Pb concentration maxima are typically consistent with a mixture of eastern and western European sources (Sherrell et al., 2000; Bazzano et al., 2015, 2021). In this study, cluster mean trajectories obtained for winter 2018-2019 highlighted a 25% of air mass provenance from Russian Arctic and a 13% from eastern Siberia (Fig. \$6), possibly explaining the higher concentrations of Pb revealed in spring 2019, following a reduced precipitation regime that occurred in January 2019. A local anthropogenic origin can be excluded though, since no activities (ordinary-extraordinary maintenance or particular events) were recorded in the vicinity of the sampling site in 2019. In addition, both GSRS and Ny-Ålesund (Fig. S2), located at 1 km of distance from each other, recorded comparable high concentrations of Pb, thus ruling out a possible contamination. However, at present, the long-range transport of Pb remains a hypothesis, likely supported by the breakdown of the wintry polar vortex (Fig. 1).

Backward trajectories (Fig. 56) for Ny-Ålesund area (78.92° N, 11.89° E) appear mostly in line with literature findings (Platt et al., 2022; Vecchiato et al., 2024), showing three main seasonal characters: a prevalent mass movement from ice-covered Central Arctic Ocean, Kara Sea, and Greenland Sea during autumn, a main provenance from Central Arctic Ocean and Kara Sea during winter, and a predominant trajectory from Northern Canada in addition to air masses arriving from Arctic Ocean and Kara seas during spring.

4.2 The main ion sources in the seasonal snow of Ny-Ålesund,

from 1.3 to 1.5 w w⁻¹, slightly lower than the expected value of 1.8 w w⁻¹ in the pure seawater (Zhuang et al., 1999), pointing the occurrence of a minimum Cl⁻ depletion in aerosol, quantified as 14% for the 2018-19 and 2019-20 campaigns, and as just 2% for the 2020-21 campaign. A possible explanation for this phenomenon could be the de-chlorination of sea-spray aerosol during transport. This reaction occurs when sea-salt particles containing NaCl interact with acids such as HNO₃, H₂SO₄, or organic acids, leading to the release of gaseous HCl (Zhuang et al., 1999, and reference therein). Although less likely, this process could also occur at the snow-atmosphere interface. On the

Examining the dominant ions associated with marine aerosol, we found Cl⁻/Na⁺ median ratios ranging

ha eliminato: European, Post-Soviet States,

ha eliminato: S8

ha eliminato: To clarify the origins of Pb peaks recorded between winter and spring 2019 further investigations are needed, which goes beyond the scope of this study.

ha eliminato: Other backward

ha eliminato: S8

ha eliminato: 4.2

ha eliminato:

Formattato: Struttura + Livello:2 + Stile numerazione: 1, 2, 3, ... + Comincia da:2 + Allineamento: A sinistra + Allinea a: 1,26 cm + Imposta un rientro di: 1,89 cm

ha eliminato: Looking at

ha eliminato: to the

ha eliminato: ,

ha eliminato: ; while

<u>contrary</u>, a possible influence of biomass burning on Cl^- depletion process has been excluded by the <u>very low</u> correlation (0.18, p value < 0.05) found between Cl^- depletion values and nss- K^+/K^+ ratios, which is a tracer of relative contribution of biomass burning (Song et al., 2018).

692

693

694

695

696

697

698

699 700

701

702

703

704

705

706

707

708

709

710

711

712

713

714

715

716

717

718

719 720

721 722

723

724

inputs.

Positive correlations between Mg, Ca, and K⁺, with Na⁺ and Cl₂ (all above 0.90, p value <0.05) suggest a common sea-spray source. However, the concentrations of Mg are also positively correlated with nss-Ca ($\rho_{load} = 0.55$), calculated according to Morales et al. (1998), indicating a shared non-marine source. This suggests that in addition to their marine origin, these ions (Mg, Ca) also have contributions from a non-marine, crustal source. Further evidence comes from the Ca/Mg ratios in surface snow samples collected during the three campaigns, which were higher than those found in seawater (0.32, Millero et al., 2008). This excess indicates the likely presence of mineral particles (i.e., calcite and dolomite), potentially originating from local rock or soil dust (e.g., limestone, dolostone, and marble, which are abundant in Svalbard), as previously observed by Barbaro et al. (2021). To further explore the mixed sources of these elements, we calculated the Enrichment Factors (EFs) of Mg and Ca. For Mg, the EF values were consistently above 10 in all the seasons analysed, indicating a significant non-crustal source (e.g., marine). In contrast, Ca displayed EF values greater than 10 only during autumn 2019, suggesting that its non-crustal contribution (likely from sea spray) was more pronounced during that specific season. Based on these findings, we conclude that Mg and Ca effectively share a common sea spray origin, but the sea-salt contribution of Ca was mainly significant in autumn 2019, while the excess of Ca in other seasons likely reflects inputs from crustal source, such as local mineral dust.

Similarly, sulphate (SO_4^2) is highly and significantly correlated (p < 0.05) with both Na⁺ ($\rho_{load} = 0.76$) and Cl⁻ ($\rho_{load} = 0.93$), indicating that sea-spray is its main source. Nonetheless, Na⁺/ $SO_4^{2^-}$ and Cl⁻/ $SO_4^{2^-}$ ratios are significantly lower than typical seawater values (3.97 and 7.13, respectively, according to Millero et al., 2008) for the former two campaigns (2018-19, 2019-20). The elevated sulphate concentrations compared to sodium, also in winter snow, suggest the absence of a strong frost flower signature. Additionally, the lack of significant depletion in nss- $SO_4^{2^-}$ further supports the minimal role of frost flowers in contributing to the snow composition. Therefore, while frost flowers are known to impact snow chemistry in Svalbard (Rankin et al., 2002; Beaudon and Moore, 2009; Roscoe et al., 2011), our analysis indicates that their contribution to the observed sea salt peaks in Kongsfjorden during the 2018-19, 2019-20 campaigns was likely limited. This analysis highlights that, while sea ice extent supports higher sea-salt concentrations in snow, the specific sulfate and ion

ha eliminato: negative

ha eliminato: appear positively correlated

ha eliminato: -, which may indicate

ha eliminato: suggesting that they share some

ha eliminato: (s). Moreover,

ha eliminato: had greater Ca: Mg ratios

ha eliminato:), pointing that the

ha eliminato: of these ions may come from

ha eliminato: derived

ha eliminato: (2021).

ha eliminato: Additionally, sulfate

ha eliminato: This

ha eliminato: an input

ratios observed point to sea spray as the main source, with only a minor role for frost flower-related

Instead, the presence of nss-SO₄² suggests potential inputs from other sources, such as crustal material, anthropogenic emissions (e.g., fossil fuel combustion), or the oxidation of dimethylsulfide (DMS) released from marine biological activities.

To estimate the crustal fraction of sulphate (cr-SO₄²⁻), the nss-Ca (as crustal marker) content was multiplied by 0.59 (SO₄²⁻/Ca w/w ratio in the uppermost Earth crust - Wagenbach et al. 1996), obtaining variable contributions for the three sampling campaigns, ranging from 2.45% up to 12.94%. Conversely, the anthropogenic contribution to nss-SO₄²⁻ concentrations was investigated by the application of the [ex- SO₄²⁻] concentration formula (Schwikowski et al., 1999), considering the average concentration of [Ca] instead of the average ionic concentration [Ca²⁺] because Ca²⁺ concentrations were not measured in the samples collected during the second campaign due to instrumental limitations:

 $[ex-SO_4^{2-}] = [SO_4^{2-}] - (0.12 [Na^+]) - (0.175 [Ca^{2+}])$

Udisti et al., 2020).

The obtained results showed a 50 up to 60% of anthropogenic contribution for the nss-SO₄²⁻ input. This finding corroborates previous results from Amore et al. (2022), who noted that anthropogenic sulphate was the most abundant apportioned component at Gruvebadet, accounting for at least 50% all over the year during the 2010-2019 investigated period. The plausible source of the anthropogenic fraction is the atmospheric transport of secondary aerosols containing SO₄²⁻, and ammonium sulphate. This sulphate can be formed by SO₂ emitted from coal combustion throughout the winter and biomass

burning in the spring (Barbaro et al., 2021 and reference therein). The nss-SO₄² does not correlate

significantly with other ionic species (except for Mg), thus suggesting a separate origin.

To quantify the biogenic nss- SO_4^{2-} contribution, the methanesulfonic acid (MSA) loads - the final product of DMS oxidation - were multiplied by 3.0 (Udisti et al., 2016), revealing biogenic SO_4^{2-} contributions ranging from 0.15% (2018-19, 2020-21) up to 0.38% (2019-20). Furthermore, the MSA/nss- SO_4^{2-} ratio was inspected, revealing a mean value of 0.02 ± 0.03 during the first (2018-19) and the third (2020-21) sampling campaigns, and a maximum ratio equal to 0.06 ± 0.18 reached during the second campaign (2019-20), similar to the subarctic western North Pacific ratio found by Jung et al. (2014). However, several factors can influence MSA formation, a univocal marker of biogenic emissions, including higher biological productivity related to higher nutrient input; the concentrations of NO_3 radicals as key oxidants for DMS decomposition (higher NO_3 gives higher

ha eliminato: -, which may originate

ha eliminato: inputs, the transport of

ha eliminato: compounds (e.g.,

ha eliminato: fuels

ha spostato (inserimento) [1]

ha spostato (inserimento) [2]

ha spostato (inserimento) [3]

ha eliminato: 2020-21

MSA); and lower air temperatures, which tend to yield higher MSA levels (Andreae et al., 1985;

For the 2019-20 campaign, it seems likely that a combination of these three factors, together with the positive expansion of sea ice and the very close drift ice presence in March 2020, as revealed from satellite reconstructions (Fig. §7), contributed to the increased release of MSA in aerosol, and its consistent deposition in surface snow (Fig. 2). Indeed, DMS was likely accumulated under the sea ice cover in the fjord and surrounding areas, and then being released and oxidised in atmosphere when the ice broke off and melted (April-May). Furthermore, lower temperatures, highly positive correlation between MSA and NO_3^- ($\rho_{load} = 0.64$), and <u>high-speed</u> short-range transport (wind directions between 0°-60° and speeds > 5 m sec⁻¹) from the source to the near-coast sink site (GSRS) would have aided elevated concentrations of MSA in atmospheric depositions. <u>However, the dominant south and southwest winds (180°-240°) during the major MSA peak in April 2020 (Fig. 2) likely transported marine aerosols and DMS from open ocean regions, further facilitating the increased MSA concentrations observed.</u>

Contrarily, in the 2018-19 season, sea ice <u>lasted only until April and was restricted to the inner, shallower parts of Kongsfjorden (Assmy et al., 2023)</u>, possibly not allowing enough time with adequate sunlight for substantial biological activity to accumulate beneath or within it. This occurred despite the dominance in 2019, unlike the following year, of *Phaeocystis pouchetii*, a phytoplankton species known for its capacity to generate DMS in significant quantities, according to Assmy et al. (2023).

Finally, the ammonium (NH₄⁺) load showed significant positive correlations with Na⁺ ($\rho_{load} = 0.76$),

C1 ($\rho_{load} = 0.62$) and K⁺ ($\rho_{load} = 0.75$), as well as with SO₄²⁻ ($\rho_{load} = 0.62$), NO₃⁻ ($\rho_{load} = 0.58$), MSA

 $(\rho_{load} = 0.52)$ and Br^{-} $(\rho_{load} = 0.62)$, suggesting a close link with sea-salt ions and biogenic emissions.

<u>However</u>, some contribution from biomass burning events <u>and potential influence from anthropogenic activities</u> cannot be excluded.

799 4.3 Bromine enrichment

776

777 778

779

780 781

782

783 784

785 786

787

788

789

790

791

792

793

794

795

796

797

798

800

801

802

803

804

805

806

The bromine enrichment factor (Br_{enr}) is well known to reflect specific processes (i.e., sea ice gas phase Br_{e} emission) that affect the Br_{e} concentration and load in the snowpack (Spolaor et al., 2014). Therefore, calculating the relative enrichment over the Br/Na ratio in sea water can offer crucial insights on sea ice variability for the investigated Arctic areas (Barbaro et al., 2021). As reported in previous studies (Maffezzoli et al., 2017; Barbaro et al., 2021), the Br_{e} enrichment factor (Br_{enr}) can be calculated as $Br_{enr} = Br_{e} / (0.0065 \ Na^{+})$, where 0.0065 represents the Br_{e}/Na^{+} seawater mass ratio. Contrarily to what observed in a former study (Barbaro et al., 2021) for the Hornsund area and north-

ha eliminato: S9

ha eliminato: the

ha eliminato: melted significantly earlier,

ha eliminato: of a species known for high DMS production

ha spostato in alto [1]: 1996), obtaining variable contributions for the three sampling campaigns, ranging from 2.45% up to 12.94%.

ha spostato in alto [2]: : 9

[ex- SO_4^2] = [SO_4^2] – (0.12 [Na^+]) – (0.175 [Ca^{2+}])¶ The obtained results showed a 50 up to 60% of anthropogenic contribution for the nss- SO_4^2 input

ha spostato in alto [3]: can be formed by SO_x emitted from coal combustion throughout the winter and biomass burning in the spring (Barbaro et al., 2021 and reference therein). The nss- SO_4 ² does not correlate significantly with other ionic species (except for Mg), thus suggesting a separate origin. \P

ha eliminato: The crustal fraction of sulfate (cr-SO₄²) was estimated by multiplying the nss-Ca (as crustal marker) content by 0.59 (SO₄²/Ca w/w ratio in the uppermost Earth crust - Wagenbach et al.

ha eliminato: ¶

The anthropogenic contribution to nss-SO₄²⁻ concentrations was also investigated by the application of the [ex-SO₄²⁻] concentration formula, considering the average concentration of [Ca] instead of the average ionic concentration [Ca²⁺] for the already clarified reason

ha eliminato:, corroborating previous results showed for the same area by Amore et al. (2022). The plausible source of the anthropogenic fraction is the atmospheric transport of secondary aerosols containing SO4²⁻, and ammonium sulfate. This sulfate

ha eliminato: The

ha eliminato: , rather than anthropogenic activities, although...

Formattato: Normale, Rientro: Sinistro: 0 cm

ha eliminato:

ha eliminato:

ha eliminato:

ha eliminato: On the contrary

western Spitsbergen, where the Br_{enr} mean values were often < 1, indicating some Br^- depletion, in this study we observed Br_{enr} mean values ranging from 1.5 up to 17.7, with the highest value associated to the second sampling campaign conducted in 2019-20, which showed the most extensive sea ice coverage. These results support the impact of the sea ice expansion and the close drift ice in the Kongsfjorden on the snow chemical composition. Indeed, newly formed sea ice releases gasphase Br_{τ} into the polar atmosphere, thus supplying an extra Br^{τ} source in addition to sea spray (Spolaor et al., 2016).

4.3 Anthropogenic and natural sources of ions and particulate trace elements

846

847

848 849

850 851

852

853

854

855

856

857

858

859

860

861

862

863

864

865

866

867

868

869

870

871

872

873

874

To complement the EFs analysis and further distinguish possible anthropogenic contributions from natural ones (marine and geogenic) for ions and particulate trace elements, a Hierarchical Cluster Analysis (HCA) method was carried out. Results of clustering (Fig. 4) clearly disentangle marine (Na⁺, Cl⁻, K⁺, NH₄⁺, SO₄²⁻, NO₃⁻, Br_s, Mg, Sr, bio-SO₄²⁻, MSA), anthropogenic (As, Co, Ag, Ba, Cd, Zn, Pb, Bi, Cr, Cu, Ni), and geogenic (nss-Ca, Tl, Li, Al, Cs, Rb, Fe, Mn, U, Be, Se, V) sources of ionic and elemental species, considering the whole sampling campaign period (2018-2021). Interestingly, nss-SO₄²⁻ is brought together with the marine cluster, suggesting that its presence is largely influenced by marine biogenic sources, alongside contributions from secondary sulfate formation in the atmosphere. This indicates that nss-SO₄²⁻, despite having a variety of sources such as human contribution or dust, is closely linked to the marine environment. One important reason for this is the emission of DMS by phytoplankton. Additionally, secondary sulfate formation may have further contributed to the nss-SO₄²⁻. Co was grouped within the anthropogenic cluster in HCA, in contrast with EFs that suggested a crustal origin. However, the errors associated with the EFs are quite high. Moreover, the trend for cobalt closely aligns with anthropogenic ones (e.g., As), while distinct trends are evident for crustal elements. Therefore, while the HCA results offer a reliable perspective on source differentiation and clustering patterns, they are best interpreted as complementary to the EF calculations rather than directly integrated with them. Incorporating EFs directly into the HCA could introduce significant inaccuracies, as EFs rely on reference element ratios that may vary and thus add complexity to the clustering process, potentially skewing the results. Consequently, HCA independently provides robust insights in this context, enhancing our understanding without the additional uncertainties that EF-based clustering might introduce.

ha eliminato:

ha eliminato: 4.4

Formattato: Struttura + Livello:2 + Stile numerazione: 1, 2, 3, ... + Comincia da:2 + Allineamento: A sinistra + Allinea a: 1,26 cm + Imposta un rientro di: 1,89 cm

ha eliminato: To

ha eliminato: 3

ha eliminato: ⁻),

ha eliminato: Mg, Ba, Bi, Cr,

ha eliminato: Co,

ha eliminato: Ca, Mn, Li, Sr

ha eliminato:

ha eliminato: biogenic MSA

ha eliminato: , likely due to the coincidence of an algal bloom event with the major deposition of anthropogenic metals in surface snow. Although winter is the most eligible season for greater deposition of impurities due to favorable atmospheric conditions, Pb, and Ni show higher concentrations

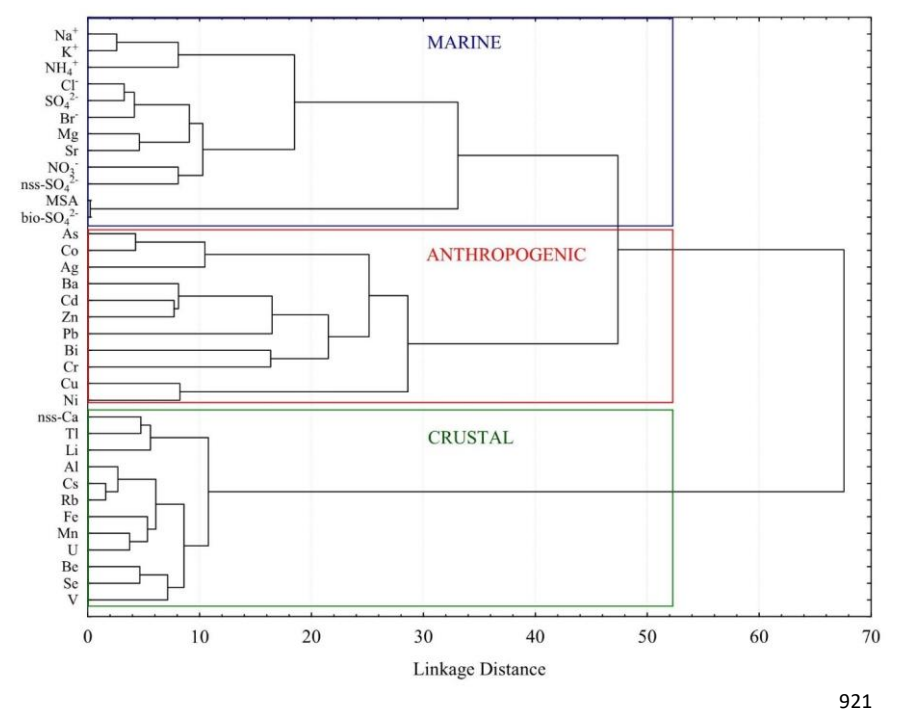
ha eliminato: spring 2019 and spring 2020, respectively (Fig. 2), representing the indicator of anomalous atmospheric and depositional events.

ha eliminato: in the absence of detailed information on the size of the particles, and on

ha eliminato: isotopic composition of

ha eliminato: investigated

ha eliminato: , which may distinguish local from longrange transport pollutants, no definitive statements can be made about the sources of these impurities.



ha eliminato: ¶ ¶ «object>

Figure 4. Hierarchical cluster analysis applied to further disentangle the particulate trace element non-crustal sources.

ha eliminato: 3

5. Summary and Conclusion

In this study, trace elements and major ions were investigated in surface snow samples collected in Ny-Ålesund between October 2018 to June 2021. Seasonal and interannual variations of impurities have been observed, with general higher concentrations of marine species revealed in late spring 2020, associated to more extensive sea ice in Kongsfjorden in March 2020, promoted by negative temperature anomalies in both atmosphere and ocean and likely related to higher air mass recycle within the Arctic. In fact, sea ice has a role in concentrating, storing, and releasing marine species, as well as influencing atmospheric and oceanic processes that affect their production and distribution. Higher concentrations in spring 2020 for geogenic and anthropogenic species were attributed instead to higher wind speeds, low atmospheric temperature anomalies, and generally drier conditions resulting from the exceptional occurrence of a strong and cold wintry stratospheric polar vortex, accompanied by an unprecedently positive phase of the Arctic Oscillation in the troposphere during January-March 2020. Therefore, our results highlighted a close dependence of high concentrations of impurities found in the snowpack at Ny-Ålesund on meteorological conditions, especially during cold

ha eliminato: Arctic type conditions, and attributed to

years, when the production of sea spray related aerosol likely derives by a larger extension of sea ice and stronger local Arctic circulation. The identification of geogenic, marine, and anthropogenic sources in the snowpack was allowed by a chemometric approach (HCA), which clarified the EFs results. The back trajectories analysis revealed distinct seasonal air mass patterns. During fall and winter, air mass predominantly originated from Northern Canada in addition to air masses arriving from Arctic Ocean and Kara seas during spring. On the contrary, no prevalent mid-latitude air currents were revealed in spring as expected, considering the period of the three sampling campaigns (2018-2021). These findings offer new insights into how specific meteorological and oceanic conditions, such as sea ice extent, wind speeds, and Arctic Oscillation phases, influence the chemical composition of the snowpack in Svalbard, particularly within the context of Arctic Amplification.

Data availability

945

946

947

948

949

950

951

952

953

954

955

956

957 958

959

960

970

971

972

The data supporting the findings of this study are available within the article and its supplementary materials. Other data that support the findings of this study are available from the corresponding author upon request.

Author contribution

AS: Conceptualization, Data curation, Investigation, Writing-original draft, Writing-review and editing. EB: Conceptualization, Field work, Data curation, Formal Analysis, Writing-original draft, 961 962 Writing-review and editing, Funding acquisition. MF: Formal Analysis, Field work, Data curation, 963 Writing-review and editing. FS: Field work, Formal analysis, Investigation, Writing-review and editing. MV: Writing-review and editing. MV: Field work, Writing-review and editing. MM: 964 Investigation. FB: Investigation, Writing-review and editing. FB: Investigation. Field work. CJMH: 965 Investigation, Data curation, Writing-review and editing. AB: Field work, Data curation, Writing-966 review and editing. AG: Resources, Supervision, Validation, Writing-review and editing, Funding 967 968 acquisition. CB: Resources, Supervision, Validation, Writing-review and editing, Funding 969 acquisition. AS: Funding acquisition, Supervision, Validation, Writing-review and editing.

Competing interests

The authors declare that they have no conflict of interest.

Acknowledgments

ha eliminato: From the comparison with previous and following seasons, the 2020-21 and 2018-19 were recognised as typical years of Arctic Amplification conditions, whilst the 2019-20 sampling campaign year has been assimilated to the Arctic type conditions. Furthermore, the

ha eliminato: brought to light an unexpected positive correlation between MSA and anthropogenic impurities during the 2020 spring season. This relation can likely be attributable to the coincidence of early spring algal bloom events with the major deposition of anthropogenic derived elements in surface snow consequent to a wintry retention of these pollutants in the atmosphere, due to a former reduced precipitation regime. Finally, back trajectories were realized, and three seasonal features were identified, with a prevalent air mass provenance from circumpolar Arctic area during fall and winter, and a predominant trajectory

ha eliminato: Our results highlight the complex interplay between atmospheric patterns, local and oceanic conditions that jointly drive snowpack impurity amounts and composition...

This project has received funding from the European Union's Horizon 2020 research and innovation programme under grant agreement no. 689443 via ERA_PLANET Strand 4 project iCUPE (Integrative and Comprehensive Understanding on Polar Environments). We are grateful to the Arctic Station Dirigibile Italia from the Italian National Research Council – Institute of Polar Science (CNR-ISP) for logistical support. The authors gratefully acknowledge Claudio Artoni, Maria Papale, Ivan Sartorato, Federico Dallo, Alice Callegaro, Marco Casula, Mariasilvia Giamberini, Fabio Giardi, and all the station leaders of "Dirigibile Italia" who participated and offered valuable help and logistic support during the 2018-2021 sampling campaigns. Furthermore, we acknowledge Klara Wolf, Linda Rehder, and Ane Kvernvik for help with CTD sampling. We acknowledge the help of ELGA LabWater in providing the PURELAB Pulse and PURELAB Flex, which produced the ultrapure water used in these experiments.

References

Amore, A., Giardi, F., Becagli, S., Caiazzo, L., Mazzola, M., Severi, M., Traversi, R.: Source apportionment of sulphate in the High Arctic by a 10 yr-long record from Gruvebadet Observatory (Ny-Ålesund, Svalbard Islands). Atmos. Environ., 270, 118890, 1-10, https://doi.org/10.1016/j.atmosenv.2021.118890, 2022

Andreae, M.O., Ferek, R.J., Bermond, F., Byrd, K.P., Engstrom, R.T., Hardin, S., Houmere, P.D., LeMarrec, F., Raemdonck, H., Chatfield, R.B.: Dimethyl sulfide in the marine atmosphere, J. Geophys. Res., 90, D7, 12891-12900, https://doi.org/10.1029/JD090iD07p12891, 1985

Assmy, P., Kvernvik, A.C., Hop, H., Hoppe, C.J.M., Chierici, M., David, D., Duarte, P., Fransson, A., Garcia, L.M., Patuła, W., Kwaśniewski, S., Maturilli, M., Pavlova, O., Tatarek, A., Wiktor, J.M., Wold, A., Wolf, K.K.E., Bailey, A.: Seasonal plankton dynamics in Kongsfjorden during two years of contrasting environmental conditions, Prog. Oceanogr., 213, 102996, https://doi.org/10.1016/j.pocean.2023.102996, 2023

Barbaro, E., Koziol, K., Björkman, M.P., Vega, C.P., Zdanowicz, C., Martma, T., Gallet, J.C., Kępski, D., Larose, C., Luks, B., Tolle, F., Schuler, T. V., Uszczyk, A., Spolaor, A.: Measurement report: Spatial variations in ionic chemistry and water-stable isotopes in the snowpack on glaciers across Svalbard during the 2015-2016 snow accumulation season, Atmos. Chem. Phys., 21, 3163–3180, https://doi.org/10.5194/acp-21-3163-2021, 2021

Barbaro, E., Padoan, S., Kirchgeorg, T., Zangrando, R., Toscano, G., Barbante, C., Gambaro, A.: Particle size distribution of inorganic and organic ions in coastal and inland Antarctic aerosol, Environ. Sci. Pollut. Res., 24, 2724-2733, https://doi.org/10.1007/s11356-016-8042-x, 2017

Barbaro, E., Zangrando, R., Vecchiato, M., Piazza, R., Cairns, W.R.L., Capodaglio, G., Barbante, C., Gambaro, A.: Free amino acids in Antarctic aerosol: Potential markers for the evolution and fate of marine aerosol, Atmos. Chem. Phys., 15, 5457–5469, https://doi.org/10.5194/acp-15-5457-2015, 2015

Codice campo modificato

Codice campo modificato

ha spostato in basso [4]: C.

ha eliminato: Barbante,

ha eliminato: Spolaor, A., Cairns, W.R., Boutron, C.: Man's footprint on the Arctic environment as revealed by analysis of ice and snow, Earth-Sci. Rev., 168, 218–231, https://doi.org/10.1016/j.earscirev.2017.02.010, 2017¶

Codice campo modificato

Codice campo modificato

Codice campo modificato

1036 Bazzano, A., Ardini, F., Becagli, S., Traversi, R., Udisti, R., Cappelletti, D., Grotti, M.: Source 1037 assessment of atmospheric lead measured at Ny-Ålesund, Svalbard, Atmos. Environ., 113, 20-26, https://doi.org/10.1016/j.atmosenv.2015.04.053, 2015 1038 Codice campo modificato Bazzano, A., Bertinetti, S., Ardini, F., Cappelletti, D., Grotti, M.: Potential Source Areas for 1039 1040 atmospheric Lead reaching Ny-Ålesund from 2010 to 2018, Atmos., 12, 388, 1-17, https://doi.org/10.3390/atmos12030388, 2021 1041 Codice campo modificato 1042 Beaudon, E., Moore, J.: Frost flower chemical signature in winter snow on Vestfonna ice cap, 1043 Nordaustlandet, Svalbard, Cryosphere, 3, 147-154, https://doi.org/10.5194/tc-3-147-2009, 2009 1044 Beine, H.J., Dominé, F., Ianniello, A., Nardino, M., Allegrini, I., Teinilä, K., Hillamo, R.: 1045 Fluxes of nitrates between snow surfaces and the atmosphere in the European high Arctic, Atmos. 1046 Chem. Phys., 3, 335-346, https://doi.org/10.5194/acp-3-335-2003, 2003 1047 Bertò, M., Cappelletti, D., Barbaro, E., Varin, C., Gallet, J.-C., Markowicz, ha spostato (inserimento) [5] 1048 Rozwadowska, A., Mazzola, M., Crocchianti, S., Poto, L., Laj, P., Barbante, C., Spolaor, A.: ha spostato (inserimento) [4] 1049 Variability in black carbon mass concentration in surface snow at Svalbard, Atmos. Chem. Phys., 21, 1050 12479-12493, https://doi.org/10.5194/acp-21-12479-2021, 2021 1051 Björkman, M., Kühnel, R., Partridge, D.G., Roberts, T.J., Aas, W., Mazzola, M., Viola, A., 1052 Hodson, A., Ström, J., Isaksson, E.: Nitrate dry deposition in Svalbard, Tellus B, 65(1), 1053 https://doi.org/10.3402/tellusb.v65i0.19071, 2013 1054 Chylek, P., Folland, C., Klett, J.D., Wang, M., Hengartner, N., Lesins, G., Dubey, M.K.: 1055 Annual Mean Arctic Amplification 1970-2020. Observed and Simulated by CMIP6 Climate Models, 1056 Geophys. Res. Lett., 49 (13), e2022GL099371, https://doi.org/10.1029/2022GL099371, 2022 Codice campo modificato 1057 D'Amico, M., Kallenborn, R., Scoto, F., Gambaro, A., Gallet, J.-C., Spolaor, A., Vecchiato, 1058 M.: Chemicals of Emerging Arctic Concern in north-western Spitsbergen snow: Distribution and 1059 sources, Sci. Total Environ., 908, 168401, https://doi.org/10.1016/j.scitotenv.2023.168401, 2024 Codice campo modificato 1060 Dethloff, K., Maslowski, W., Hendricks, S., Lee, Y.J., Goessling, H.F., Krumpen, T., Haas, 1061 C., Handorf, D., Ricker, R., Bessnov, V., Cassano, J.J., Kinney, J.C., Osinski, R., Rex, M., Rinke, A., 1062 Sokolova, J., Sommerfeld, A.: Arctic sea ice anomalies during the MOSAiC winter 2019/20, Cryosphere, 16, 981-1005, https://doi.org/10.5194/tc-16-981-2022, 2022 1063 Codice campo modificato 1064 Draxler, R.R.: An overview of the HYSPLIT_4 modelling system for trajectories, dispersion ha eliminato: Dommergue, A., Larose, C., Faïn, X., Clarisse, O., Foucher, D., Hintelmann, H., Schneider, D., and deposition, Aust. Meteorol. Mag., 47, 295-308, 1998 1065 Ferrari, C.P.: Deposition of mercury species in the Ny-Ålesund area (79°N) and their transfer during snowmelt, Eleftheriadis, K., Vratolis, S., Nyeki, S.: Aerosol black carbon in the European Arctic: 1066 Environ. Sci. Technol., 44, 901-907, 1067 Measurements at Zeppelin station, Ny-Ålesund, Svalbard from 1998-2007, Geophys. Res. Lett., 36, $https://doi.org/10.1021/es902579m,\,2010\P$ $1\!-\!5, \underline{https://doi.org/10.1029/2008GL035741}, 2009$ 1068 Codice campo modificato Feltracco, M., Barbaro, E., Hoppe, C.J.M., Wolf, K.K.E., Spolaor, A., Layton, R., Keuschnig, 1069 1070 C., Barbante, C., Gambaro, A., Larose, C.: Airborne bacteria and particulate chemistry capture Phytoplankton bloom dynamics in an Arctic fjord, Atmos. Environ., 256, 118458, 1071 1072 https://doi.org/10.1016/j.atmosenv.2021.118458, 2021 Codice campo modificato 1073 Feltracco, M., Barbaro, E., Tedeschi, S., Spolaor, A., Turetta, C., Vecchiato, M., Morabito, ha formattato: Inglese (Stati Uniti) 1074 E., Zangrando, R., Barbante, C., Gambaro, A.: Interannual variability of sugars in Arctic aerosol:

1075

1076

Biomass

burning

and

https://doi.org/10.1016/j.scitotenv.2019.136089, 2020

biogenic

inputs,

23

Sci.

Total

Environ.,

Codice campo modificato

1083 1084 1085	Geng, H., Ryu, J., Jung, H.J., Chung, H., Ahn, K.H.O., Ro, C.U.N.: Single-particle characterization of summertime arctic aerosols collected at Ny-Ålesund, Svalbard, Environ. Sci. Technol., 44, 2348–2353, https://doi.org/10.1021/es903268j, 2010	Codice campo modificato
1086 1087 1088	George, B.J., Gains-Germain, L., Broms, K., Black, K., Furman, M., Hays, M.D., Thomas, K.W., Simmons, J.E.: Censoring trace-level environmental data: statistical analysis considerations to limit bias, Environ. Sci. Technol., 55(6), 3786-3795, https://doi.org/10.1021/acs.est.0c02256, 2021	Codice campo modificato
1089 1090 1091 1092	Gerland, S., Pavlova, O., Marnela, M., Divine, D.V., Kohler, J., Renner, A., Skoglund, A.: Sea ice extent variability in Kongsfjorden, Svalbard during 2003-2021, based on visual observations from the mountain Zeppelinfjellet, Norwegian Polar Institute, https://doi.org/10.21334/npolar.2022.d6d31f5b, 2022	Codice campo modificato
1093 1094 1095 1096 1097	Gjermundsen, A., Seland Graff, L., Bentsen, M., Anders Breivik, L., Boldingh Debernard, J., Makkonen, R., Olivié, D.J.L., Seland, Ø., Zieger, P., Schulz, M.: How representative is Svalbard for future Arctic climate evolution? An Earth system modelling perspective (SvalCLIM), SESS Report 2020 – The State of Environmental Science in Svalbard, https://doi.org/10.5281/zenodo.4034104, 2020	Codice campo modificato
1098 1099 1100 1101	Hansen, B.B., Isaksen, K., Benestad, R.E., Kohler, J., Pedersen, Å., Loe, L.E., Coulson, S.J., Larsen, J.O., Varpe, Ø.: Warmer and wetter winters: Characteristics and implications of an extreme weather event in the High Arctic, Environ. Res. Lett., 9, https://doi.org/10.1088/1748-9326/9/11/114021 , 2014	Codice campo modificato
1102 1103	Hodgkins, R., Tranter, M.: Solute in High Arctic glacier snow cover and its impact on runoff chemistry, Ann. Glaciol., 26, 156-160, https://doi.org/10.3189/1998AoG26-1-156-160, 1998	ha formattato: Inglese (Regno Unito)
1104 1105 1106 1107	Jacobi, HW., Obleitner, F., Da Costa, S., Ginot, P., Eleftheriadis, K., Aas, W., Zanatta, M.:Deposition of ionic species and black carbon to the Arctic snowpack: combining snow pitobservations with modeling, Atmos. Chem. Phys., 19, 10361-10377,https://doi.org/10.3402/tellusb.v65i0.19071, 2019	Codice campo modificato
1108 1109	Jung, J., Furutani, H., Uematsu, M., Park, J.: Distributions of atmospheric non-sea-salt sulphate and methanesulfonic acid over the Pacific Ocean between 48°N and 55°S during summer,	 ha eliminato: sulfate
1110 1111 1112	Atmos. Environ., 99, 374-384, https://doi.org/10.1016/j.atmosenv.2014.10.009, 2014 Koziol, K., Uszczyk, A., Pawlak, F., Frankowski, M., Polkowska, Ż.: Seasonal and Spatial Differences in Metal and Metalloid Concentrations in the Snow Cover of Hansbreen, Svalbard, Front.	Codice campo modificato
1113 1114 1115	Earth Sci., 8, 1–8, https://doi.org/10.3389/feart.2020.538762, 2021 Lai, A.M., Shafer, M.M., Dibb, J.E., Polashenski, C.M., Schauer, J.J.: Elements and inorganic ions as source tracers in recent Greenland snow, Atmos. Environ., 164, 205–215,	Codice campo modificato
1116	https://doi.org/10.1016/j.atmosenv.2017.05.048, 2017	 Codice campo modificato
1117 1118 1119 1120	Lawrence, Z.D., Perlwitz, J., Butler, A.H., Manney, G.L., Newman, P.A., Lee, S.H., Nash, E.R.: The Remarkably Strong Arctic Stratospheric Polar Vortex of Winter 2020: Links to Record-Breaking Arctic Oscillation and Ozone Loss, J. Geophys. Res. Atmos., 125, 1–21, https://doi.org/10.1029/2020JD033271, 2020	Codice campo modificato
1121 1122	Maffezzoli, N., Spolaor, A., Barbante, C., Bertò, M., Frezzotti, M., Vallelonga, P.: Bromine, iodine and sodium in surface snow along the 2013 Talos Dome-GV7 traverse (northern Victoria Land,	
1123	East Antarctica), Cryosphere, 11, 693-705, https://doi.org/10.5194/tc-11-693-2017, 2017	 Codice campo modificato

Millero, F.J., Feistel, R., Wright, D.G., McDougall, T.J.: The composition of Standard Seawater and the definition of the Reference-Composition Salinity Scale, Deep-Sea Res., 55, 50–72, 2008

1128

1129

1130

1131

1132

1133

1134

1135

1136

1137

1138

1139

1140

1141

1142

1143

1144

1145

1146

1147

1148

1149 1150

1151

1152

1153

1154 1155

1156

1157

1158

1159 1160

1161

1162

1163

Morales, J.A., Pirela, D., de Nava, M.G., de Borrego, B.S., Velásquez, H., Durán, J.: Inorganic water soluble ions in atmospheric particles over Maracaibo Lake Basin in the western region of Venezuela, Atmos., Res., 46, https://doi.org/10.1016/S0169-8095(97)00071-9, 1998

Nawrot, A.P., Migała, K., Luks, B., Pakszys, P., Głowacki, P.: Chemistry of snow cover and acidic snowfall during a season with a high level of air pollution on the Hans Glacier, Spitsbergen, Polar Sci., 10, 249–261, https://doi.org/10.1016/j.polar.2016.06.003, 2016

Platt, S.M., Hov, Ø., Berg, T., Breivik, K., Eckhardt, S., Eleftheriadis, K., Evangeliou, N., Fiebig, M., Fisher, R., Hansen, G., Hansson, H.-C., Heintzenberg, J., Hermansen, O., Heslin-Rees, D., Holmén, K., Hudson, S., Kallenborn, R., Krejci, R., Krognes, T., Larssen, S., Lowry, D., Lund Myhre, C., Lunder, C., Nisbet, E., Nizzetto, P.B., Park, K.-T., Pedersen, C.A., Pfaffhuber, K.A., Röckmann, T., Schmidbauer, N., Solberg, S., Stohl, A., Ström, J., Svendby, T., Tunved, P., Tørnkvist, K., van der Veen, C., Vratolis, S., Yoon, Y.L., Yttri, K.E., Zieger, P., Aas, W., Tørseth, K.: Atmospheric composition in the European Arctic and 30 years of the Zeppelin Observatory, Ny-Ålesund, Atmos. Chem. Phys., 22, 3321-3369, https://doi.org/10.5194/acp-22-3321-2022, 2022

Pomeroy, J.W.: A process-based model of snow drifting, Ann. Glaciol., 13, 237-240, https://doi.org/10.3189/S0260305500007965, 1989

Rankin, A.M., Wolff, E.W.: Frost flowers: Implications for tropospheric chemistry and ice core interpretation, J. Geophys. Res., 107, D23, 4683, https://doi.org/10.1029/2002JD002492, 2002

Rantanen, M., Karpechko, A.Y., Lipponen, A., Nordling, K., Hyvärinen, O., Ruosteenoja, K., Vihma, T., Laaksonen, A.: The Arctic has warmed nearly four times faster than the globe since 1979, Commun. Earth Environ, 3, 168, https://doi.org/10.1038/s43247-022-00498-3, 2022

Rinke, A., Maturilli, M., Graham, R.M., Matthes, H., Handorf, D., Cohen, L., Hudson, S.R., Moore, J.C.: Extreme cyclone events in the Arctic: Wintertime variability and trends, Environ. Res. Lett., 12, https://doi.org/10.1088/1748-9326/aa7def, 2017

Roscoe, H.K., Brooks, B., Jackson, A.V., Smith, M.H., Walker, S.J., Obbard, R.W., Wolff, E.W.: Frost flowers in the laboratory: Growth, characteristics, aerosol, and the underlying sea ice, J. Geophys. Res., 116, D12301, https://doi.org/10.1029/2010JD015144, 2011

Ruppel, M.M., Khedr, M., Liu, X., Beaudon, E., Szidat, S., Tunved, P., Ström, J., Koponen, H., Sippula, O., Isaksson, E., Gallet, J.-C., Hermanson, M., Manninen, S., Schnelle-Kreis, J.: Organic compounds, radiocarbon, trace elements and atmospheric transport illuminating sources of elemental carbon in a 300-year Svalbard ice core, J. Geophys. Res.: Atmos., 128, https://doi.org/10.1029/2022JD038378, 2023

Salzano, R., Cerrato, R., Scoto, F., Spolaor, A., Valentini, E., Salvadore, M., Esposito, G., Sapio, S., Taramelli, A., Salvatori, R.: Detection of winter heat wave impact on surface runoff in a periglacial environment (Ny-Ålesund, Svalbard), Remote Sens., 15(18), 4435, https://doi.org/10.3390/rs15184435, 2023

ha formattato: Inglese (Regno Unito)

Codice campo modificato

ha eliminato: Paatero, J., Buyukay, M., Holmén, K., Hatakka, J., Viisanen, Y.: Seasonal variation and source areas of airborne lead-210 at Ny-Ålesund in the High Arctic, Polar

ha eliminato: 29, 345-352, https://doi.org/10.3402/polar.v29i3.6085, 2010¶ Pilguj, N., Kolendowicz, L., Kryza, M., Migala, K., Czernecki, B.: Temporal changes in wind conditions at Svalbard for the years 1986-2015, Geografiska Annaler: Series A, Physical Geography, https://doi.org/10.1080/04353676.2019.1572973, 2019¶

ha formattato: Inglese (Regno Unito)

Codice campo modificato

Codice campo modificato

Codice campo modificato

Codice campo modificato

1174	Schoeberl, M.R., Newman, P.A.: Middle Atmosphere: Polar Vortex, Encyclopedia of		
1175	Atmospheric Sciences, Second Edition, Elsevier, 12-17, https://doi.org/10.1016/B978-0-12-382225-		Codice campo modificato
1176	3.00228-0, 2015		
1177	Schwikowski, M., Döscher, A., Gäggeler, H.W., Schotterer, U.: Anthropogenic versus natural		
1178	sources of atmospheric sulphate from an Alpine ice core. Tellus B: Chemical and Physical		
1179	Meteorology, 51:5, 938-951, https://doi.org/10.3402/tellusb.v51i5.16506, 1999		
l 1180	Scoto, F., Pappaccogli, G., Mazzola, M., Donateo, A., Salzano, R., Monzali, M., de Blasi, F.,		
1181	Larose, C., Gallet, JC., Decesari, S., Spolaor, A.: Automated observation of physical snowpack		
1182	properties in Ny-Ålesund, Front. Earth Sci., 11:1123981, 1-9, https://doi.org/		
1183	0.3389/feart.2023.1123981, 2023		
1184	Serreze, M.C., Barry, R.G.: Processes and impacts of Arctic amplification: A research		
1185	synthesis, Glob. Planet. Change, 77, 85-96, http://dx.doi.org/10.1016/j.gloplacha.2011.03.004, 2011		Codice campo modificato
			Courte cumpo mounicato
1186	Sherrell, R.M., Boyle, E.A., Harris, N.R., Falkner, K.K.: Temporal variability of Cd, Pb, and Pb isotope deposition in central Greenland snow, Geochem Geophys, 1 (1), 1-22,		
1187 1188	https://doi.org/10.1029/1999GC000007, 2000		Codice campo modificato
			Cource campo mounicato
1189	Sobota, I., Weckwerth, P., Grajewski, T.: Rain-On-Snow (ROS) events and their relations to		
1190 1191	snowpack and ice layer changes on small glaciers in Svalbard, the high Arctic, J. Hydrol, 590, 125279, https://doi.org/10.1016/j.jhydrol.2020.125279, 2020		C. P. C.
			Codice campo modificato
1192	Song, C., Becagli, S., Beddows, D.C.S., Brean, J., Browse, J., Dai, Q., Dall'Osto, M., Ferracci,		
1193	V., Harrison, R.M., Harris, N., Li, W., Jones, A.E., Kirchgäßner, A., Kramawijaya, A.G., Kurganskiy,		
1194 1195	A., Lupi, A., Mazzola, M., Severi, M., Traversi, R., Shi, Z.: Understanding sources and drivers of size-resolved aerosol in the High Arctic islands of Svalbard using a receptor model coupled with		
1196	machine learning, Environ. Sci. Technol., 56, 11189-11198, https://doi.org/10.1021/acs.est.1c07796,		Codice campo modificato
1197	2022		Course campo mounicato
1100	Song I 7hoo V 7hong V Ey D 7hong I Vyon O Wong S Hyong V Vy W Coo		
1198 1199	Song, J., Zhao, Y., Zhang, Y., Fu, P., Zheng, L., Yuan, Q., Wang, S., Huang, X., Xu, W., Cao, Z., Gromov, S., Lai, S.: Investigation of biomass burning on atmospheric aerosols over the western		
1200	South China Sea: Insights from ions, carbonaceous fractions and stable carbon isotope ratios,		
1201	Environ. Pollut., 242, 1800-1809, https://doi.org/10.1016/j.envpol.2018.07.088, 2018		Codice campo modificato
1202	Spolaor, A., Scoto, F., Larose, C., Barbaro, E., Burgay, F., Bjorkman, M., Cappelletti, D.,		
1202	Dallo, F., de Blasi, F., Divine, D., Dreossi, G., Gabrieli, J., Isaksson, E., Kohler, J., Martma, T.,		
1204	Schmidt, L.S., Schuler, T.V., Stenni, B., Turetta, C., Luks, B., Casado, M., Gallet, JC.: Climate		
1205	change is rapidly deteriorating the climatic signal in Svalbard glaciers, Cryosphere, 18, 307-320,		
1206	https://doi.org/10.5194/tc-18-307-2024, 2024		Codice campo modificato
1207	Spolaor, A., Varin, C., Pedeli, X., Christille, J.M., Kirchgeorg, T., Giardi, F., Cappelletti, D.,		
1208	Turetta, C., Cairns, W.R.L., Gambaro, A., Bernagozzi, A., Gallet, J.C., Björkman, M.P., Barbaro, E.:		
1209	Source, timing and dynamics of ionic species mobility in the Svalbard annual snowpack, Sci. Total		
1210	Environ., 751, 141640, https://doi.org/10.1016/j.scitotenv.2020.141640, 2021b		Codice campo modificato
1211	Spolaor, A., Moroni, B., Luks, B., Nawrot, A., Roman, M., Larose, C., Stachnik, Ł., Bruschi,		
1212	F., Kozioł, K., Pawlak, F., Turetta, C., Barbaro, E., Gallet, JC., Cappelletti, D.: Investigation on the		
1213	Sources and Impact of Trace Elements in the Annual Snowpack and the Firn in the Hansbreen		
1214	(Southwest Spitsbergen), Front. Earth Sci., 8, 1–10, https://doi.org/10.3389/feart.2020.536036, 2021a		Codice campo modificato

1217 Lopez, A., Barbante, C., Cairns, W.R.L.: Diurnal cycle of iodine, bromine, and mercury 1218 concentrations in Svalbard surface snow, Atmos. Chem. Phys., 19, 13325-13339, 1219 https://doi.org/10.5194/acp-19-13325-2019, 2019 Codice campo modificato 1220 Spolaor, A., Angot, H., Roman, M., Dommergue, A., Scarchilli, C., Vardè, M., Del Guasta, 1221 M., Pedeli, X., Varin, C., Sprovieri, F., Magand, O., Legrand, M., Barbante, C., Cairns, W.R.L: 1222 Feedback mechanisms between snow and atmospheric mercury: Results and observations from field 1223 campaigns on the Antarctic plateau, Chemosphere, 1224 https://doi.org/10.1016/j.chemosphere.2017.12.180, 2018 Codice campo modificato 1225 Spolaor, A., Opel, T., McConnell, J.R., Maselli, O.J., Spreen, G., Varin, C., Kirchgeorg, T., Fritzsche, D., Saiz-Lopez, A., Vallelonga, P.: Halogen-based reconstruction of Russian Arctic sea ice 1226 area from the Akedemii Nauk ice core (Severnaya Zemlya), Cryosphere, 10, 245-256, 1227 https://doi.org/10.5194/tc-10-245-2016, 2016 1228 Codice campo modificato Spolaor, A., Vallelonga, P., Gabrieli, J., Martma, T., Björkman, M.P., Isaksson, E., Cozzi, G., 1229 Turetta, C., Kjær, H.A., Curran, M.A.J., Moy, A.D., Schönhardt, A., Blechschmidt, A.-M., Burrows, 1230 1231 J.P., Plane, J.M.C., Barbante, C.: Seasonality of halogen deposition in polar snow and ice, Atmos. Chem. Phys., 14, 18, 9613-9622, https://doi.org/10.5194/acp-14-9613-2014, 2014 1232 Codice campo modificato 1233 Stein, A.F., Draxler, R.R., Rolph, G.D., Stunder, B.J.B., Cohen, M.D., Ngan, F.: Noaa's ha spostato in alto [5]: ., Varin, C. 1234 hysplit atmospheric transport and dispersion modeling system, Bull. Am. Meteorol. Soc., 96, 2059ha eliminato: Spolaor, A., Gabrieli, J., Martma, T., Kohler, J., Björkman, M.B., Isaksson, E 1235 2077, https://doi.org/10.1175/BAMS-D-14-00110.1, 2015 ha eliminato: Vallelonga, P., Plane, J.M.C., Barbante, C.: Stohl, A., Berg, T., Burkhart, J.F., Fjæraa, a. M., Forster, C., Herber, A., Hov, Ø., Lunder, C., 1236 Sea ice dynamics influence halogen deposition to Svalbard, Cryosphere, 7, 1645-1658, https://doi.org/10.5194/tc-7-1645-McMillan, W.W., Oltmans, S., Shiobara, M., Simpson, D., Solberg, S., Stebel, K., Ström, J., Tørseth, 1237 2013, 2013¶ K., Treffeisen, R., Virkkunen, K., Yttri, K.E.: Arctic smoke - record high air pollution levels in the 1238 Codice campo modificato European Arctic due to agricultural fires in Eastern Europe, Atmos. Chem. Phys. Discuss., 6, 9655-1239 9722, https://doi.org/10.5194/acpd-6-9655-2006, 2006b 1240 Codice campo modificato 1241 Stohl, A., Berg, T., Burkhart, J.F., Fjæraa, a. M., Forster, C., Herber, A., Hov, Ø., Lunder, C., 1242 McMillan, W.W., Oltmans, S., Shiobara, M., Simpson, D., Solberg, S., Stebel, K., Ström, J., Tørseth, K., Treffeisen, R., Virkkunen, K., Yttri, K.E.: Arctic smoke - record high air pollution levels in the 1243 European Arctic due to agricultural fires in Eastern Europe, Atmos. Chem. Phys. Discuss., 6, 9655-1244 1245 9722, https://doi.org/10.5194/acpd-6-9655-2006, 2006a Codice campo modificato 1246 Turetta, C., Feltracco, M., Barbaro, E., Spolaor, A., Barbante, C., Gambaro, A.: A year-round 1247 measurement of water-soluble trace and rare earth elements in arctic aerosol: Possible inorganic 1248 tracers of specific events, Atmosphere, 12, https://doi.org/10.3390/atmos12060694, 2021 Codice campo modificato Udisti, R., Traversi, R., Becagli, S., Tomasi, C., Mazzola, M., Lupi, A., Quinn, P.K.: Arctic 1249 Aerosols, in: Physics and Chemistry of the Arctic Atmosphere, Springer Polar Sciences, edited by: 1250 1251 Kokhanovsky, A., Tomasi, C., 209-329, https://doi.org/10.1007/978-3-030-33566-3_4, 2020 Codice campo modificato 1252 Udisti, R., Bazzano, A., Becagli, S., Bolzacchini, E., Caiazzo, L., Cappelletti, D., Ferrero, L.,

ha eliminato: Sulfate

Spolaor, A., Barbaro, E., Cappelletti, D., Turetta, C., Mazzola, M., Giardi, F., Björkman, M.P.,

Lucchetta, F., Dallo, F., Aspmo Pfaffhuber, K., Angot, H., Dommergue, A., Maturilli, M., Saiz-

Frosini, D., Giardi, F., Grotti, M., Lupi, A., Malandrino, M., Mazzola, M., Moroni, B., Severi, M.,

Traversi, R., Viola, A., Vitale, V.: Sulphate source apportionment in the Ny-Ålesund (Svalbard

Islands) Arctic aerosol, Rend. Fis. Acc. Lincei, 27, Suppl 1: S85-S94, https://doi.org/10.1007/s12210-

1215

1216

1253

1254

1255 1256

016-0517-7, 2016

1265 1266 1267 1268 1269	Vecchiato, M., Barbante, C., Barbaro, E., Burgay, F., Cairns, W.R.L., Callegaro, A., Cappelletti, D., Dallo, F., D'Amico, M., Feltracco, M., Gallet JC., Gambaro, A., Larose, C., Maffezzoli, N., Mazzola, M., Sartorato, I., Scoto, F., Turetta, C., Vardè, M., Xie, Z., Spolaor, A.: The seasonal change of PAHs in Svalbard surface snow, Environ. Pollut., 340, 122864, https://doi.org/10.1016/j.envpol.2023.122864, 2024	Codice campo modificato
1270 1271 1272	Vecchiato, M., Barbaro, E., Spolaor, A., Burgay, F., Barbante, C., Piazza, R., Gambaro, A.: Fragrances and PAHs in snow and seawater of Ny-Ålesund (Svalbard): Loca and long-range contamination, Environ. Pollut., 242, 1740-1747, https://doi.org/10.1016/j.envpol.2018.07.095, 2018	 Codice campo modificato
1273 1274 1275 1276 1277	Vega, C.P., Björkman, M.P., Pohjola, V.A., Isaksson, E., Pettersson, R., Martma, T., Marca, A., Kaiser, J., Vega, C.P., Björkman, M.P., Pohjola, V.A., Isaksson, E., Pettersson, R., Martma, T., Marca, A., Kaiser, J., Pohjola, V.A., Isaksson, E., Pettersson, R., Vega, C.P., Bjo, M.P.: Nitrate stable isotopes and major ions in snow and ice samples from four Svalbard sites Nitrate stable isotopes and major ions in snow and ice samples from four Svalbard sites, Polar Res., 2015, 34, 23246,	
1278 1279 1280 1281	https://doi.org/10.3402/polar.v34.23246, 2015 Wagenbach, D., Preunkert, S., Schäfer, J., Jung, W., Tomadin, L.: Northward transport of Saharan dust recorded in a deep alpine ice core, in: The impact of desert dust across the mediterranean, Springer, The Netherlands, edited by: Guerzoni, S., Chester, R., 291-300, 1996	Codice campo modificato
1282 1283	Wedepohl, K.H.: The composition of the chemical crust. Geoch. Cosm. Act., 59(7), 1217-1232, https://doi.org/10.1016/0016-7037(95)00038-2, 1995	
1284 1285 1286 1287	Yttri, K.E., Lund Myhre, C., Eckhardt, S., Fiebig, M., Dye, C., Hirdman, D., Ström, J., Klimont, Z., Stohl, A.: Quantifying black carbon from biomass burning by means of levoglucosan - A one-year time series at the Arctic observatory Zeppelin, Atmos. Chem. Phys., 14, 6427–6442, https://doi.org/10.5194/acp-14-6427-2014, 2014a	
1288 1289 1290	Zhan, J., Gao, Y., Li, W., Chen, L., Lin, H., Lin, Q.: Effects of ship emissions on summertime aerosols at Ny-Alesund in the Arctic, Atmos. Pollut. Res., 5, 500–510, https://doi.org/10.5094/APR.2014.059, 2014	Codice campo modificato Codice campo modificato
1291 1292	Zhuang, H., Chan, C.K., Fang, M., Wexler, A.S.: Size distributions of particulate <u>sulphate</u> , nitrate, and ammonium at a coastal site in Hong Kong, Atmos. Environ., 33, 843-853, 1999	 ha eliminato: sulfate
1293		
1294		